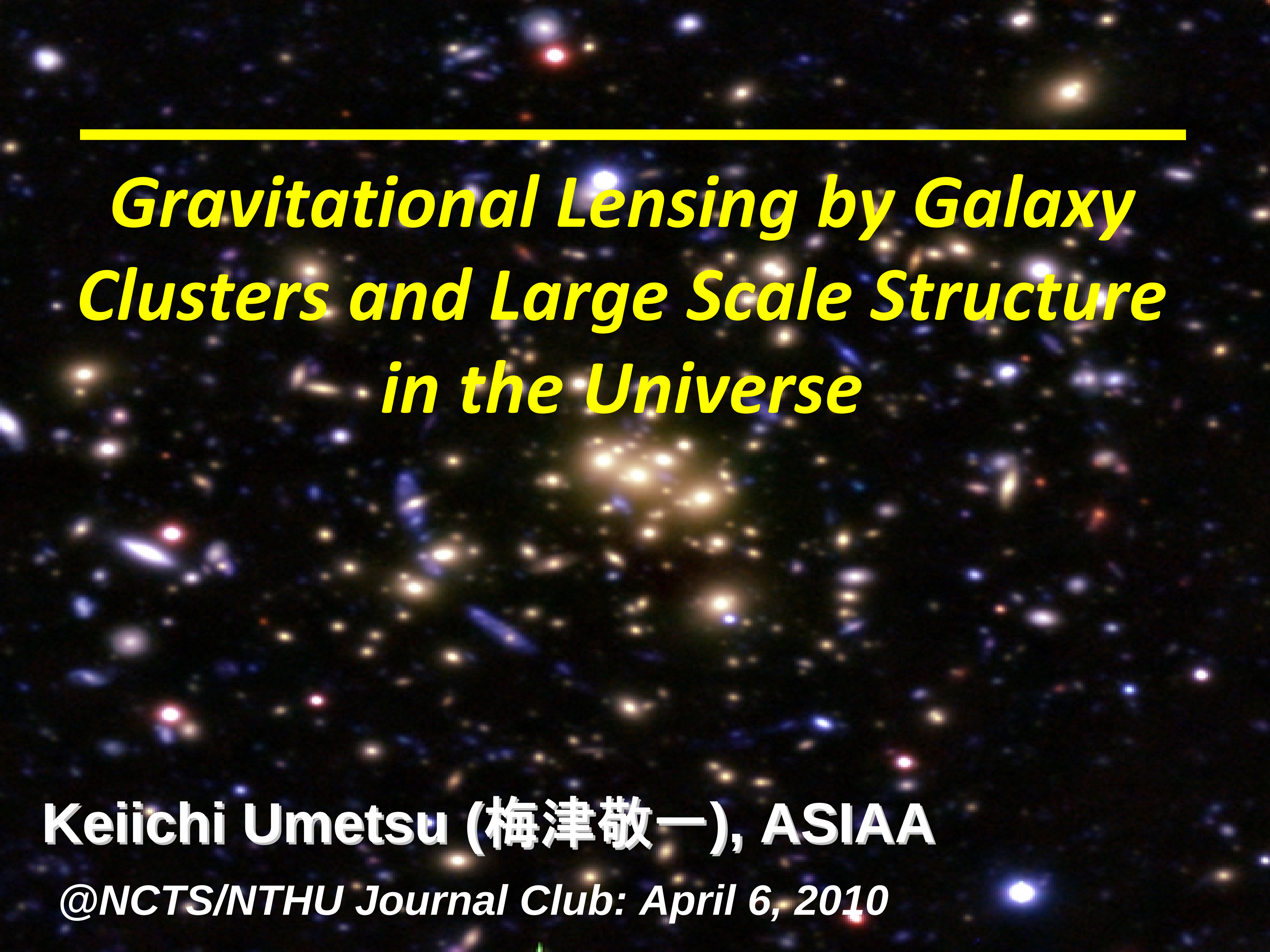

Gravitational Lensing by Galaxy Clusters and Large Scale Structure in the Universe

Keiichi Umetsu (梅津敬一), ASIAA

@NCTS/NTHU Journal Club: April 6, 2010

Collaborators (this talk)

Tom Broadhurst (Tel Aviv U., Israel)
Elinor Medezinski (Tel Aviv U., Israel)
Adi Zitrin (Tel Aviv U., Israel)
Yoel Rephaeli (Tel Aviv U., Israel)
Nobuhiro Okabe (ASIAA, Taiwan)
Sandor Molnar (ASIAA, Taiwan)
Bau-Ching Hsieh (ASIAA, Taiwan)
Masahiro Takada (IPMU, Japan)
Toshifumi Futamase (Tohoku U., Japan)
Masamune Oguri (NAOJ, Japan)
Graham P. Smith (Birmingham U., UK)

Contents

1. Equilibrium Density Profile of Dark Matter Halos

Concordance Structure Formation Scenario

Standard Lambda Cold Dark Matter (=LCDM) Paradigm:

– **Initial conditions**, precisely known from linear theory & CMB$^+$ data (@ $z = z_{dec} \sim 1100$)

– >70% of the current energy density is in the form of mysterious DE.

– ~85% of our *material universe* is composed of DM

– Use an **N-body simulation** (+linear theory) to study hierarchical structure formation ($0 < z < 1100$)

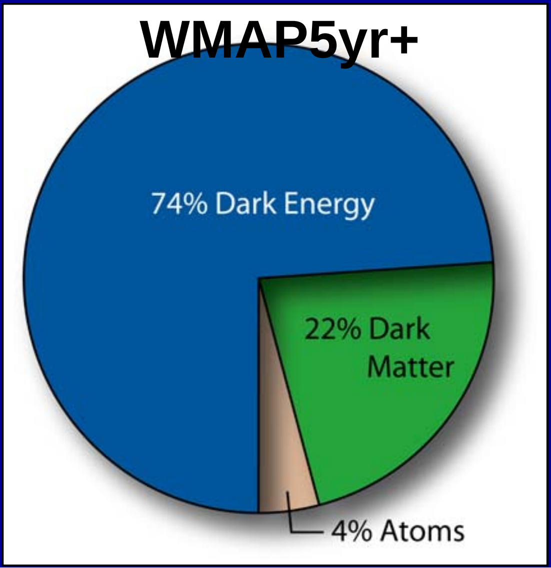

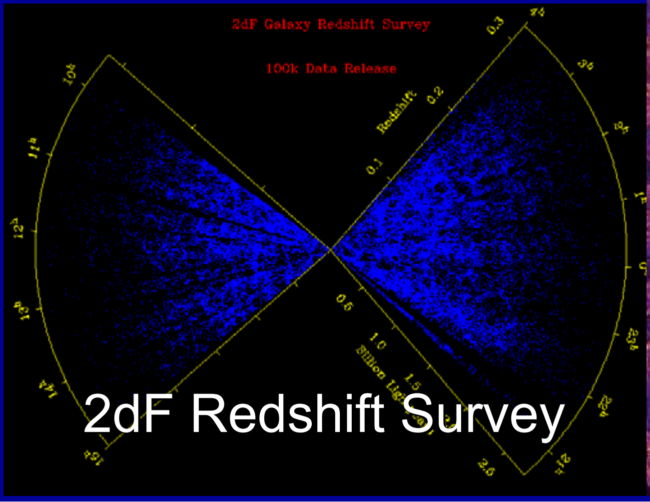

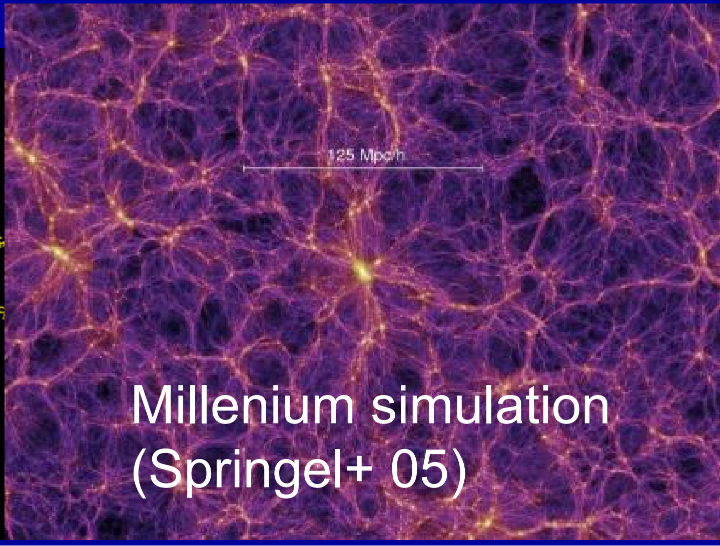

Nature of CDM Structure Formation

1. **Hierarchical growth**: Non-relativisitc (cold) nature of DM
   – bottom up formation of structures in the CDM model
   – smaller objects first form, and merge together into larger systems: i.e., galaxies -> groups -> clusters -> superclusters
2. **Anisotropic collapse**: Collisionless nature of DM
   – any small initial deviation from sphericity of a collapsing cloud gets magnified by tidal forces (e.g., Zel'dovich 1970; Shen et al. 2006)
   – gravitational collapse proceeds along sequence:
     - Collapse along smallest axis -> planar geometry ->wall
     - Collapse along middle axis -> filament
     - Collapse along longest axis -> triaxial (spheroidal) DM halos

After having collapsed into a clump, "virialization and emergence" of cosmic object

3. **Void formation**: δ ~ "-1" nonlinear structure
   – Under-dense regions, corresponding to density troughs in primordial density fields

Observed Matter P(k) vs. LCDM

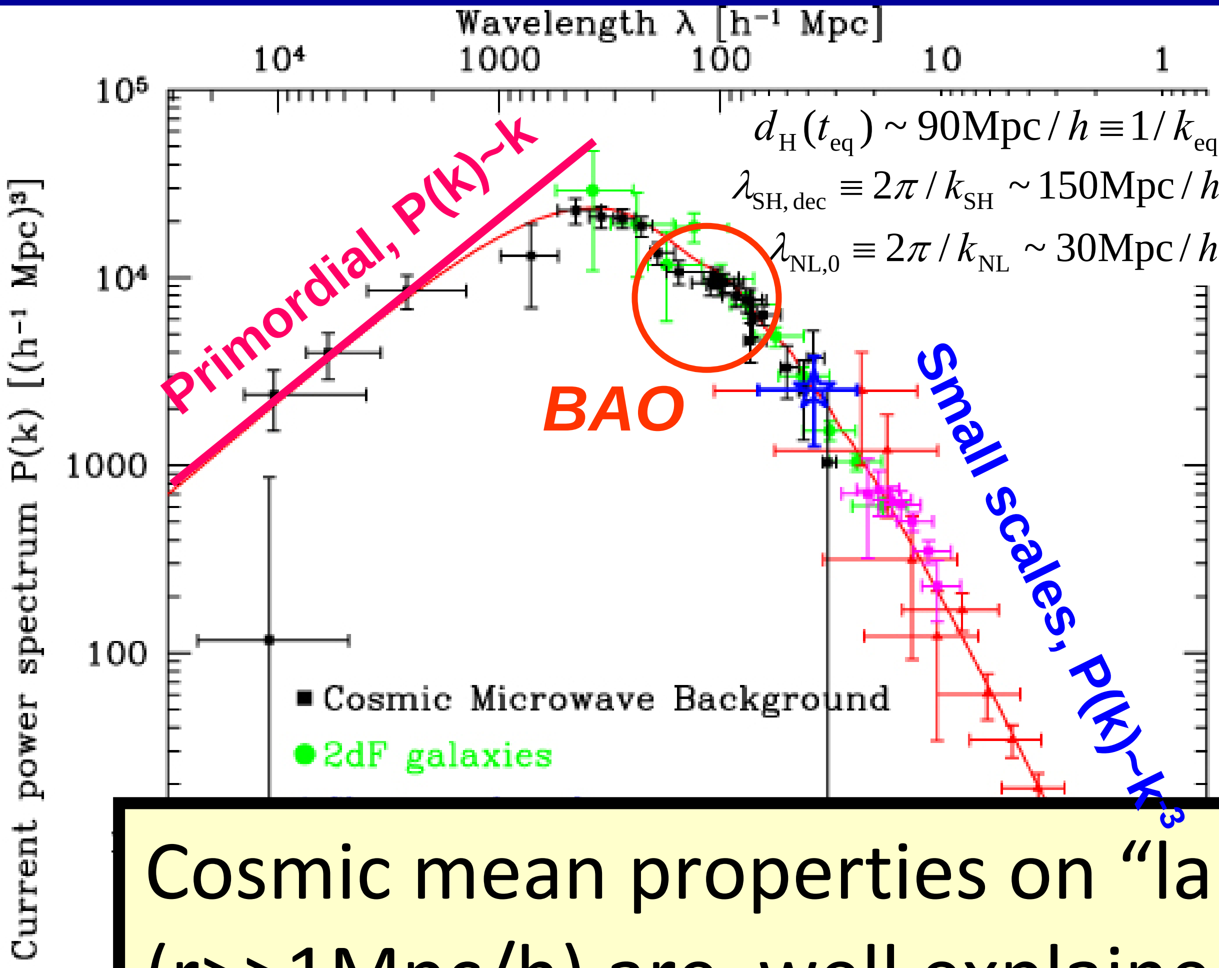

Tegmark & Zaldarriaga 2002

P(k) = A k^n with n ~ 1 @ k<< k_{eq}~0.01h/Mpc

Turn-over @ k~k_{eq}

P(k)=Ak^(n-4) @ k>>k_{eq} due to decay of Φ(k) on sub-horizon scales in the radiation era

Baryon acoustic oscillation (BAO) features

...es,

...z=0,

with σ(k_{NL})~1

Cosmic mean properties on "large scales" (r>>1Mpc/h) are well explained by ΛCDM. How about nonlinear scales (<1-10Mpc/h)?

Gravitational Growth of Structure: Gravitational Instability

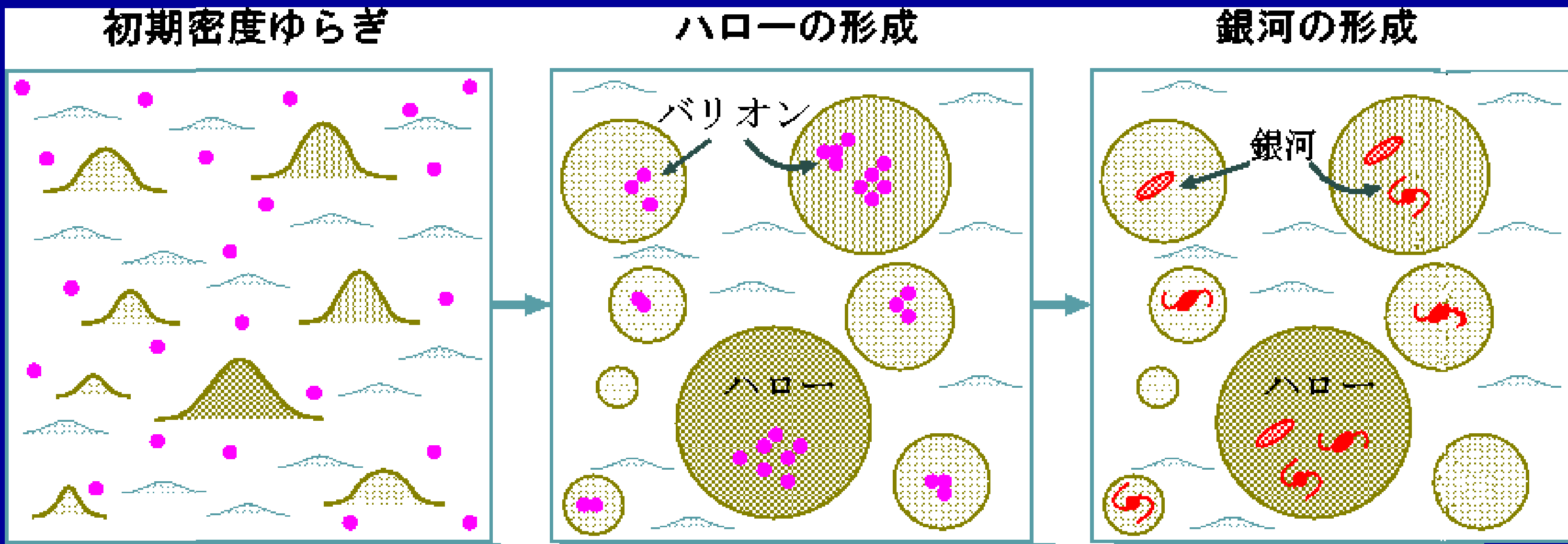

Growth of density perturbations

Gas cooling, radiative process, SF etc.

DM halo formation via gravitational collapse

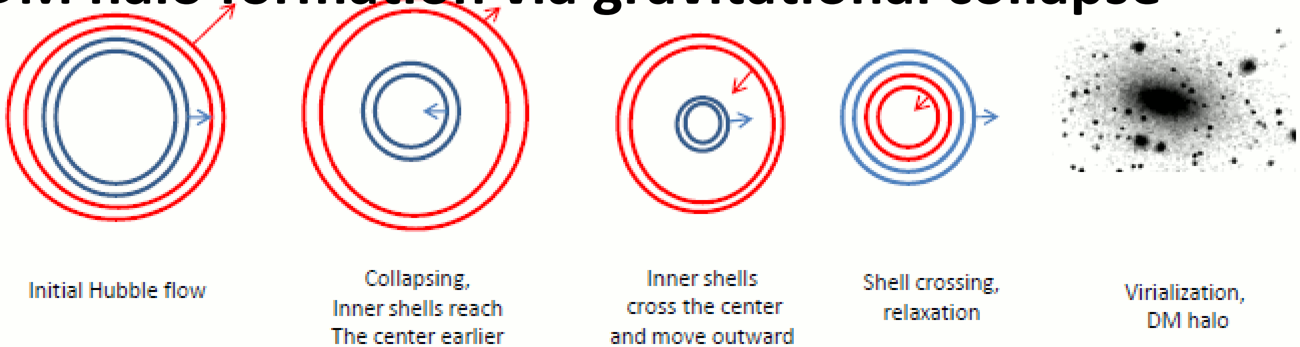

Overdense regions:

Hubble flow
→ Turn around
→ Violent relaxation
→ Mass acretion, hierarchical mergers

Simulated Gravitational Instability

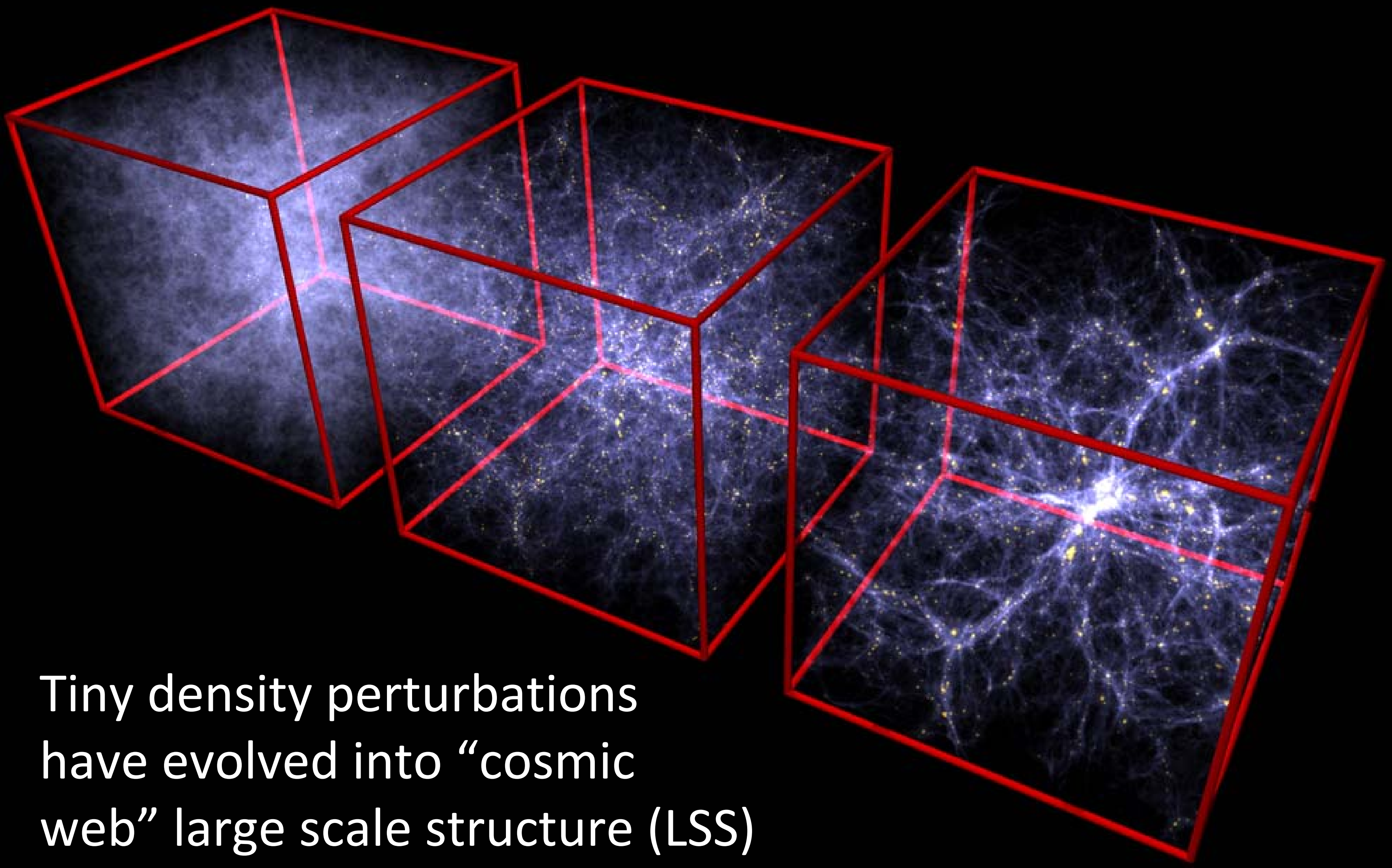

Tiny density perturbations have evolved into "cosmic web" large scale structure (LSS)

Large Scale Structure and Galaxy Clusters

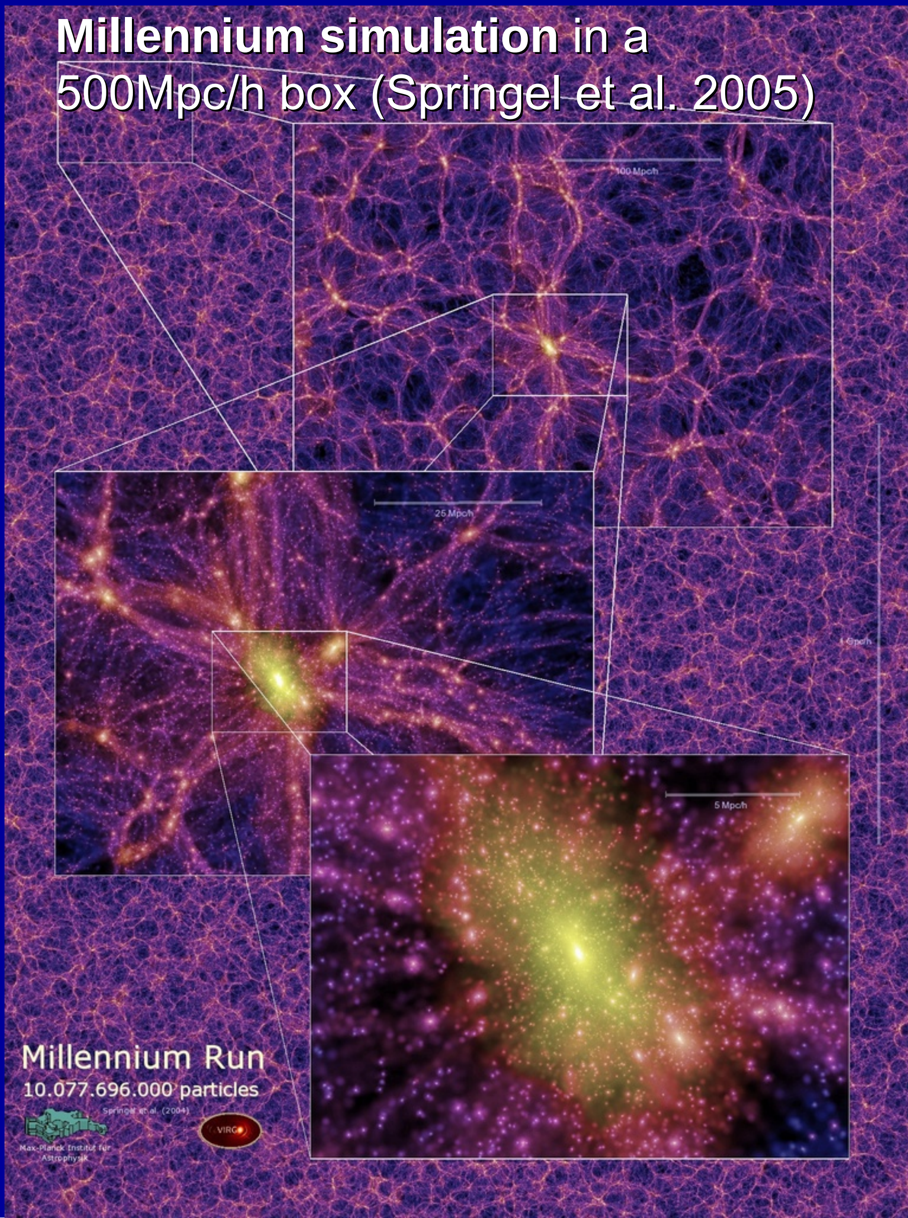

Millennium simulation in a 500Mpc/h box (Springel et al. 2005)

N-body simulations

Study "nonlinear" structure formation in an expanding Universe after the cosmic decoupling epoch (z~1100) governed by the *gravity*

- Large Scale Structure: cosmic structure on scales of ~10-50 Mpc/h in mildly-nonlinear regime (δ~1), representing forming superclusters, low-density voids, filaments of galaxies.

- Clusters of galaxies: largest self-gravitating systems (aka, DM halos) with δ>>1, composed of $10^{2\text{-}3}$ galaxies.

$$M_{vir} \sim 10^{14-15} M_{\rm sun}/h$$

$$R_{vir} \sim 1-2{\rm Mpc}/h \;\Rightarrow\; t_{dyn} = 3-5{\rm Gyr} < {\rm t_H}$$

$$k_{\rm B} T_{gas} \sim 5-10{\rm keV}$$

Simulated Clusters of Galaxies

Galaxy Clusters – identified as dense nodes of "Cosmic Web", being building blocks of LSS

Distribution of discrete **galaxies** (N=$10^{2\text{-}3}$) Distribution of underlying **DM** (~mass)

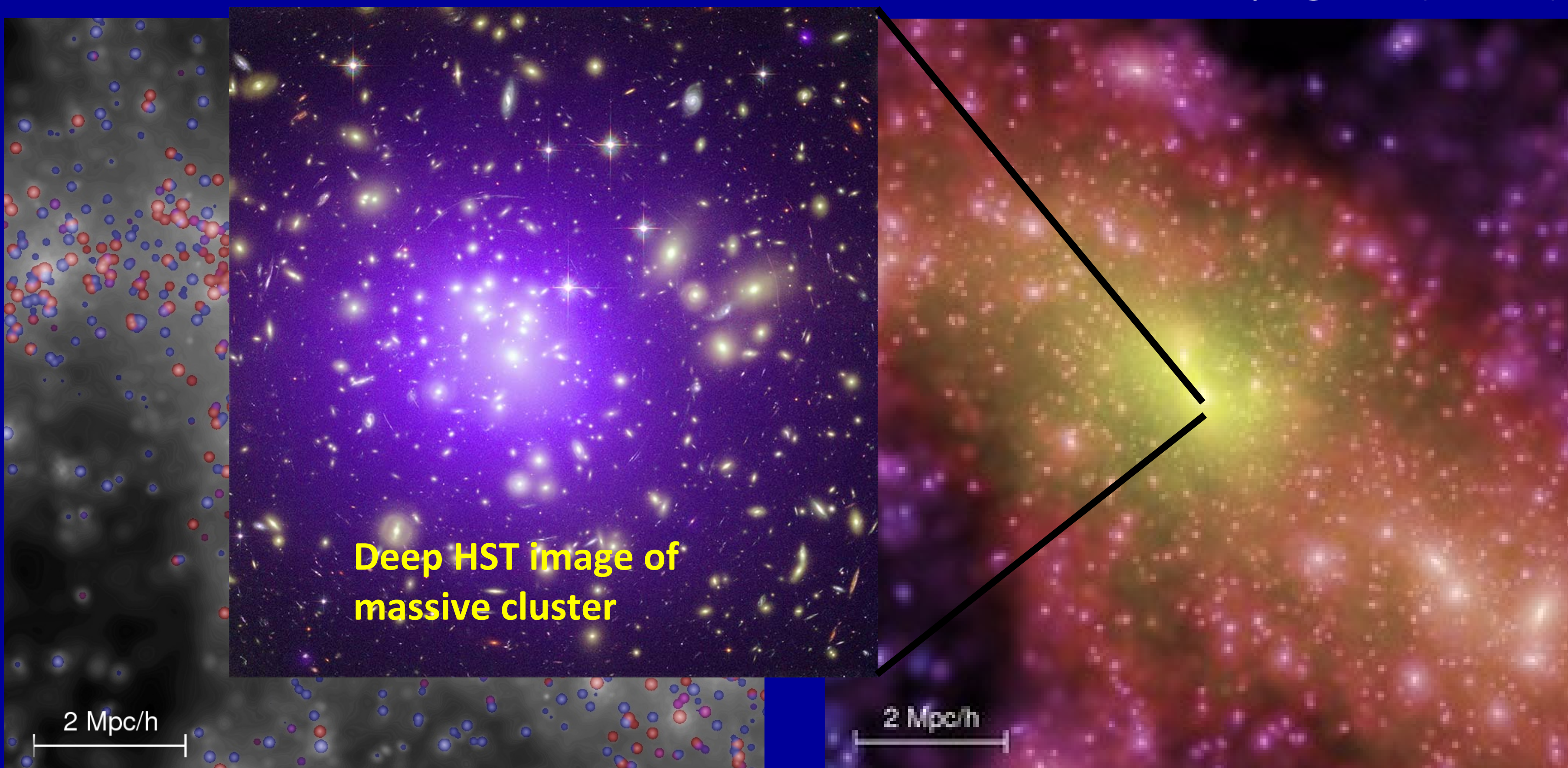

From Millennium Simulation DM distribution around a forming cluster

Clusters as

A1689 (z=0.18

- *Subaru*
  Suprime-C
  34’x27’
- *HST ACS*
  3.3’x3.3’
- *Chandra* ACI
- AMiBA
- VLT/VIRMOS
- Suzaku/XIS

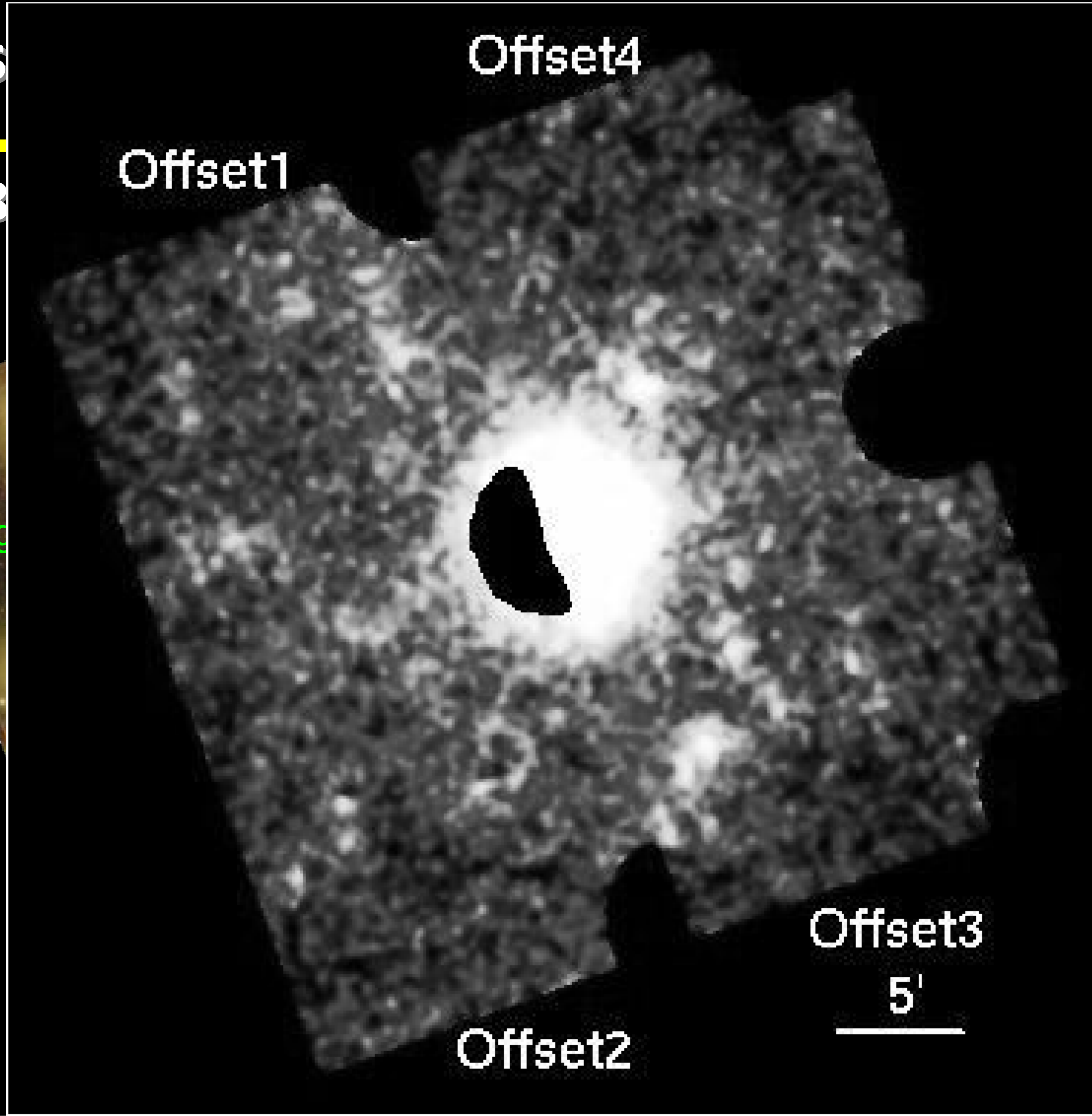

Unresolved Problem: Equilibrium Density Profile of DM Halos?

- **Theoretical interest**: ***what is the final state of the cosmological self-gravitating system ?***
  - **Forget cosmological initial conditions but reflect the nature of DM (EoS, collisional nature)?**
  - **Keep initial memory somehow?**
- **Practical importance**: ***testable predictions for galaxies and galaxy clusters***
  - **can distinguish the underlying cosmological model through comparison with observations: i.e., galactic rotation curve, gravitational lensing, X-ray/Sunyaev-Zel'dovich effects**

Theoretical Difficulties

- Nonlinear and N-body gravitational "relaxation" process
  - Needs numerical simulations
- Cosmological initial conditions
  - Background cosmology (Hubble flow, linear growth rate)
  - Shape and normalization of primordial matter power spectrum, $P(k) \propto k^n$
- Internal and velocity structures
  - Dynamical friction and tidal disruption of substructures in the central high-density region → Needs high mass/force resolution
  - Velocity anisotropy couples with the density profile via the Jean equation
- Cosmological boundary conditions
  - DM halos are NOT isolated systems
    - Turn around → violent virialization → 2ndary infall, mergers
  - Collisions and mergers of DM halo
  - continuous acretion of matter in outskirts from LSS → needs a wide dynamic range

Theoretical Studies (70'-90')

- **1970**: **Peebles**; N-body simulation (N=300).
- **1977**: **Gott**; secondary infall model $\rho \propto r^{-9/4}$.
- **1985**: **Hoffman & Shaham**; predict that density profile around density peaks is $\rho \propto r^{-3(n+3)/(n+4)}$.
- **1986**: **Quinn, Salmon & Zurek**; N-body simulations (N $\sim 10^4$), confirmed $\rho \propto r^{-3(n+3)/(n+4)}$.
- **1988**: **Frenk, White, Davis & Efstathiou**; N-body simulations (N=323), showed that CDM model can reproduce the flat rotation curve out to 100kpc.
- **1990**: **Hernquist**; proposed an analytic model with a central cusp for elliptical galaxies $\rho \propto r^{-1}(r+rs)^{-3}$.

Slide taken from Prof. Yasushi Suto's presentation

Concordance Universal CDM Density Profile: Navarro-Frenk-White 1997 (NFW) Model

<u>Empirical predictions</u> from cosmological N-body simulations of CDM structure formation: **"NFW" universal density profile**

— The universal profile fits DM halos that span ~9 orders of magnitude in mass (dwarf galaxies to clusters) regardless of the initial conditions and cosmology.

— Not a single power-law but continuously steepening density profile with radius: central cusp slope of n(r)=–dlnρ/dlnr=1 – 1.5 (cuspy but shallower than the isothermal body, n=2), outskirt slope of n(r)=3

$$\rho(r)/\rho_s = (r/r_s)^{-1}(1+r/r_s)^{-2}$$

$$c_{vir} := r_{vir}/r_s$$

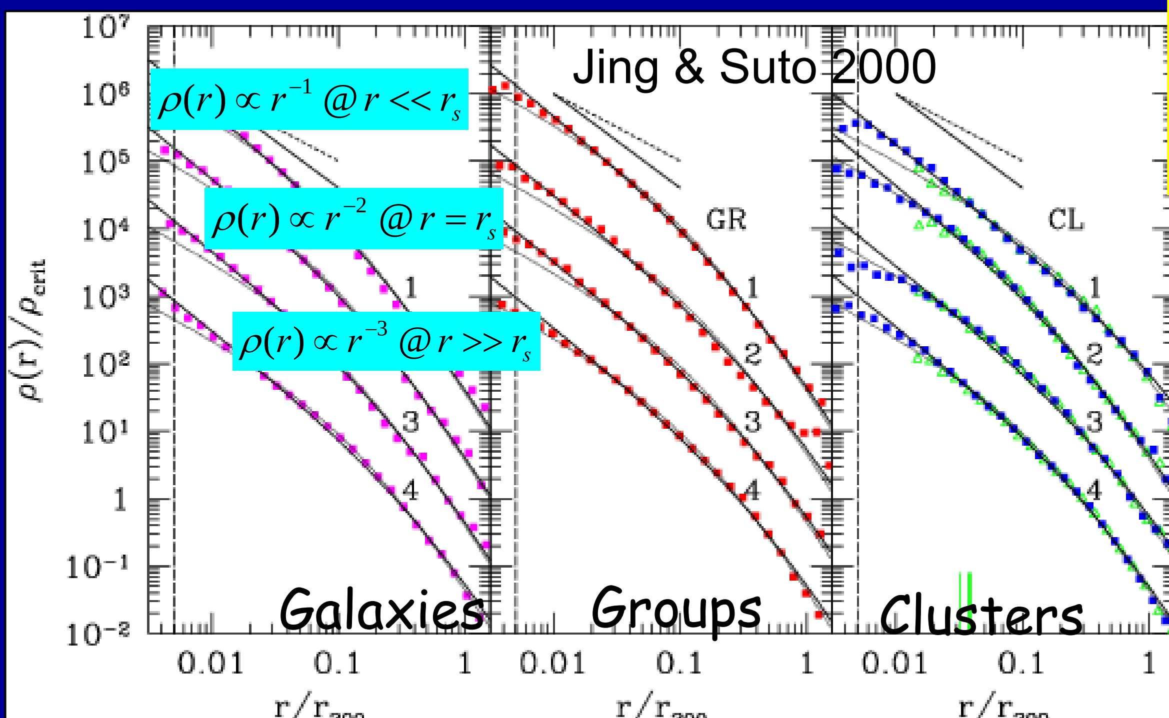

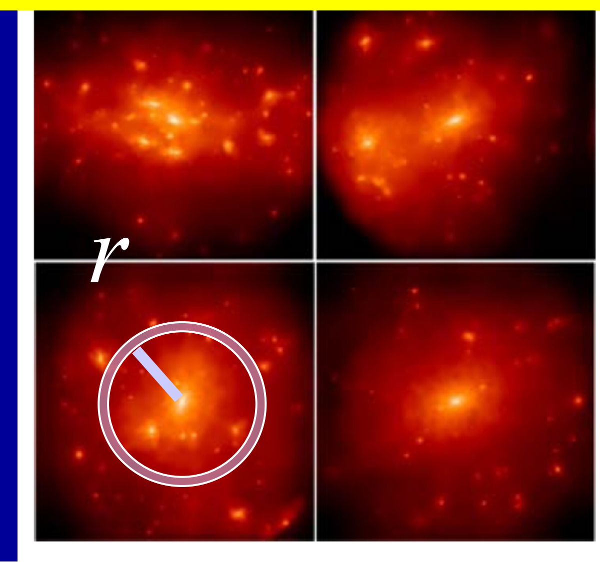

LCDM Prediction for Halo Mass vs. Concentration Correlation

Gravity is scale free – but the **formation epoch** of **DM halos**, which depends on the structure formation scenario, P(k), gives a **mass & redshift dependence of the degree of mass concentration, C_{vir}.**

LCDM N-body halo concentration vs. M_{vir} relation: $c_{vir} := r_{vir}/r_s$

$$\langle c_{\rm vir} \rangle = c_0 (1+z)^{-\alpha} \left(\frac{M_{\rm vir}}{10^{15} M_{\rm sun}/h} \right)^{-\beta}$$

$C_0 \sim 5$

$\alpha \sim 1$

$\beta \sim 0.1$

- **Spherical collapse model**: $r_{vir} \sim (1+z_{vir})^{-1}$; massive objects formed later in LCDM, so **lower concentrations for massive objects**

Bullock+2001: $\alpha=1$

Duffy+2008: $\alpha=0.66$

- Scaling radius depends on the structure formation, especially on the **formation epoch of the progenitor DM halo**

Latest LCDM Prediction: Duffy+2008

Median C-M relation of N-body CDM halos in the WMAP5 cosmology (σ_8=0.8)

$$\langle c_{\rm vir} \rangle = 5.2(1+z)^{-0.66} \left(\frac{M_{\rm vir}}{10^{15} M_{\rm sun}/h} \right)^{-0.084}$$

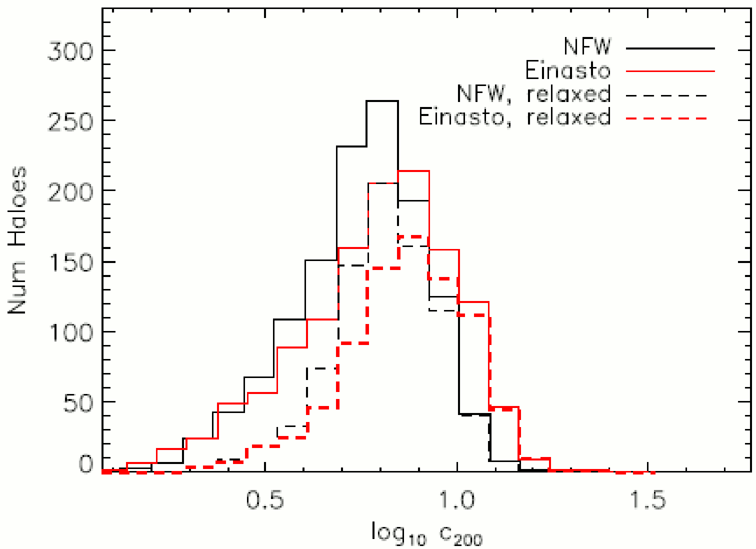

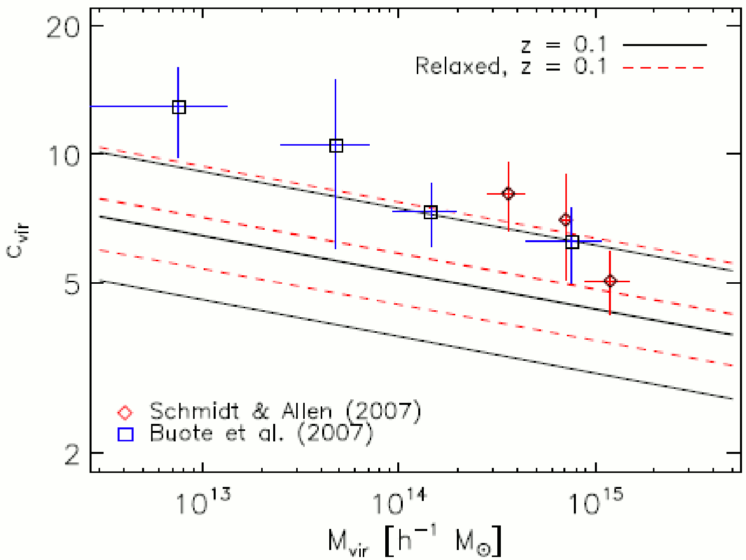

Duffy et al. 2008

My Observational Approach

- **Target: massive clusters with M_{vir}~[5-30] x 10^{14} M_{sun}/h**
  - Curvature in the density profile shape is more pronounced due to their lower mass concentration: $C_{vir} \propto M_{vir}^{-0.1}$
  - Best observational constraints are available by virtue of their high total mass.
  - Gas cooling and relevant baryonic phyisical processes are only important at r < 0.01 r_{vir} (~20kpc/h), and hot baryons (~95% of the baryons in high-mass clusters) trace the gravitational potential field dominated by DM.
- **Method: weak and strong gravitational lensing**
  - Depends only on gravity.
  - No assumption required about the physical/dynamical state of the system (cf. X-ray and dynamical observations).
  - Strong lensing provides tight constraints on the inner mass profile at r = [0.01 – 0.1] x $r_{vir.}$
  - Weak gravitational Lensing probes the cluster mass out to beyond the virial radius, r >0.1 r_{vir}, in a model independent manner.

2. Gravitational Lensing Theory

My lecture notes on

"**Cluster Weak Gravitational Lensing**"

from "Enrico-Fermi Summer School 2008, Italy" found @

arXiv:1002.3952

Theoretical backgrounds and basic concepts on cosmological lensing and observational techniques are summarized in these lecture notes.

Importance of Gravitational Lensing

Gravitationally-lensed images of background galaxies carry the imprint of $\Phi(x)$ of intervening cosmic structures:

Observable weak shape distortions can be used to derive the distribution of matter (i.e., mass) in a model independent way!!

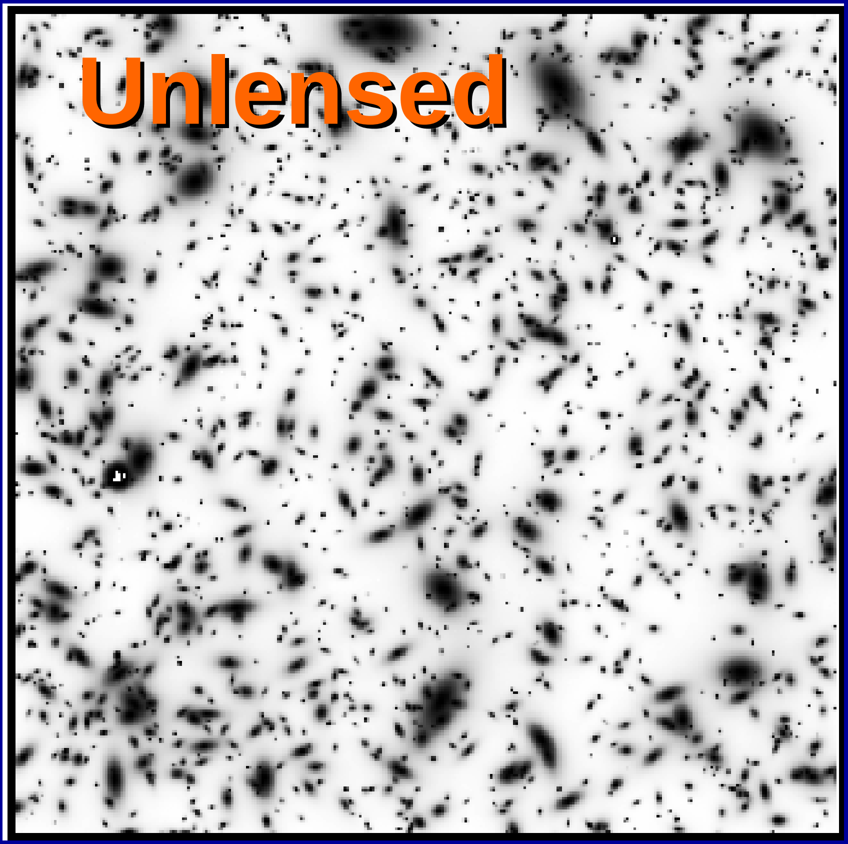

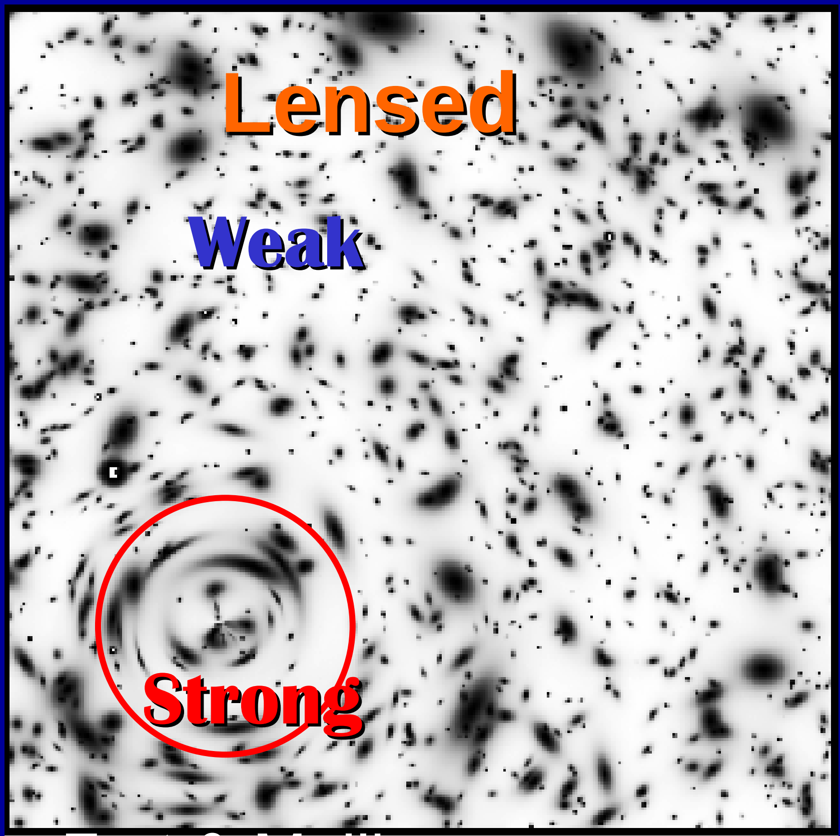

Fort & Mellier

Gravitational Bending of Light Rays

Gravitational deflection angle in the weak-field limit (|Φ|/c^2<<1)

Light rays propagating in an inhomogeneous universe will undergo **small transverse excursions** along the photon path: i.e., **light deflections**

Bending angle

$$\delta\hat{\alpha} \approx \frac{\delta p_{\perp}}{p_{\|}} = -\frac{2}{c^2}\nabla_{\perp}\Psi(x_{\|}, x_{\perp})\delta x_{\|}$$

Small transverse excursion of photon momentum

$$\hat{\alpha}^{\mathrm{GR}} = 2\hat{\alpha}^{\mathrm{Newton}} \rightarrow \frac{4GM}{c^2 r} = 1.''75\left(\frac{M}{M_{sun}}\right)\left(\frac{r}{R_{sun}}\right)^{-1}$$

Lens Equation (for cluster lensing)

Lens equation (Cosmological lens eq. + single/thin-lens approx.)

β: true (but unknown) source position

θ: apparent image position

$$\boldsymbol{\beta} - \boldsymbol{\theta} = \frac{D_{LS}}{D_{OS}} \hat{\boldsymbol{\alpha}}(\boldsymbol{\theta}) \equiv -\nabla \psi(\boldsymbol{\theta})$$

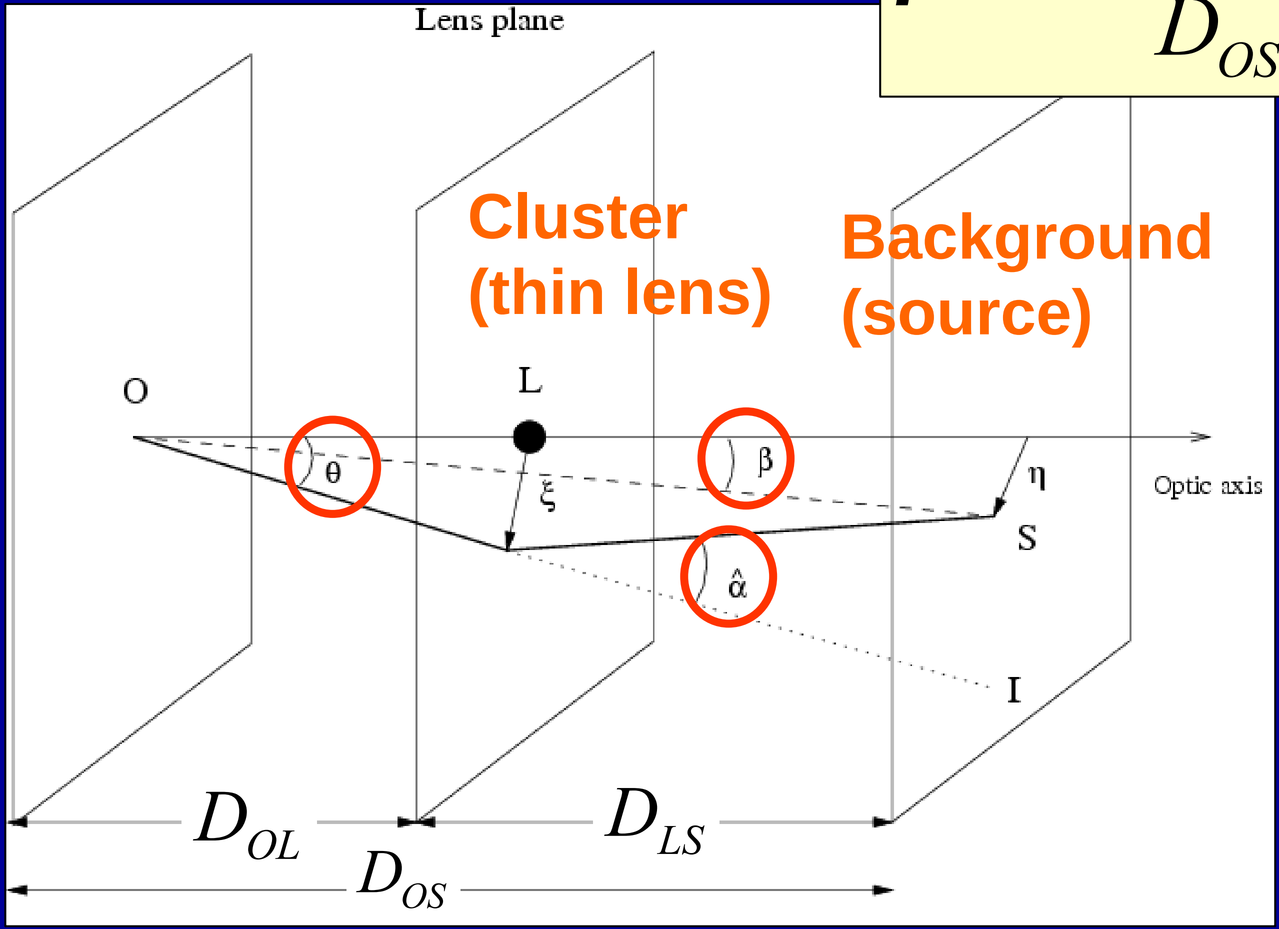

D_{OL}, D_{LS}, D_{OS} ~ $O(c/H_0)$

For a rigid derivation of cosmological lens eq., see, e.g., Futamase 95

Gravitational Lensing in Galaxy Clusters

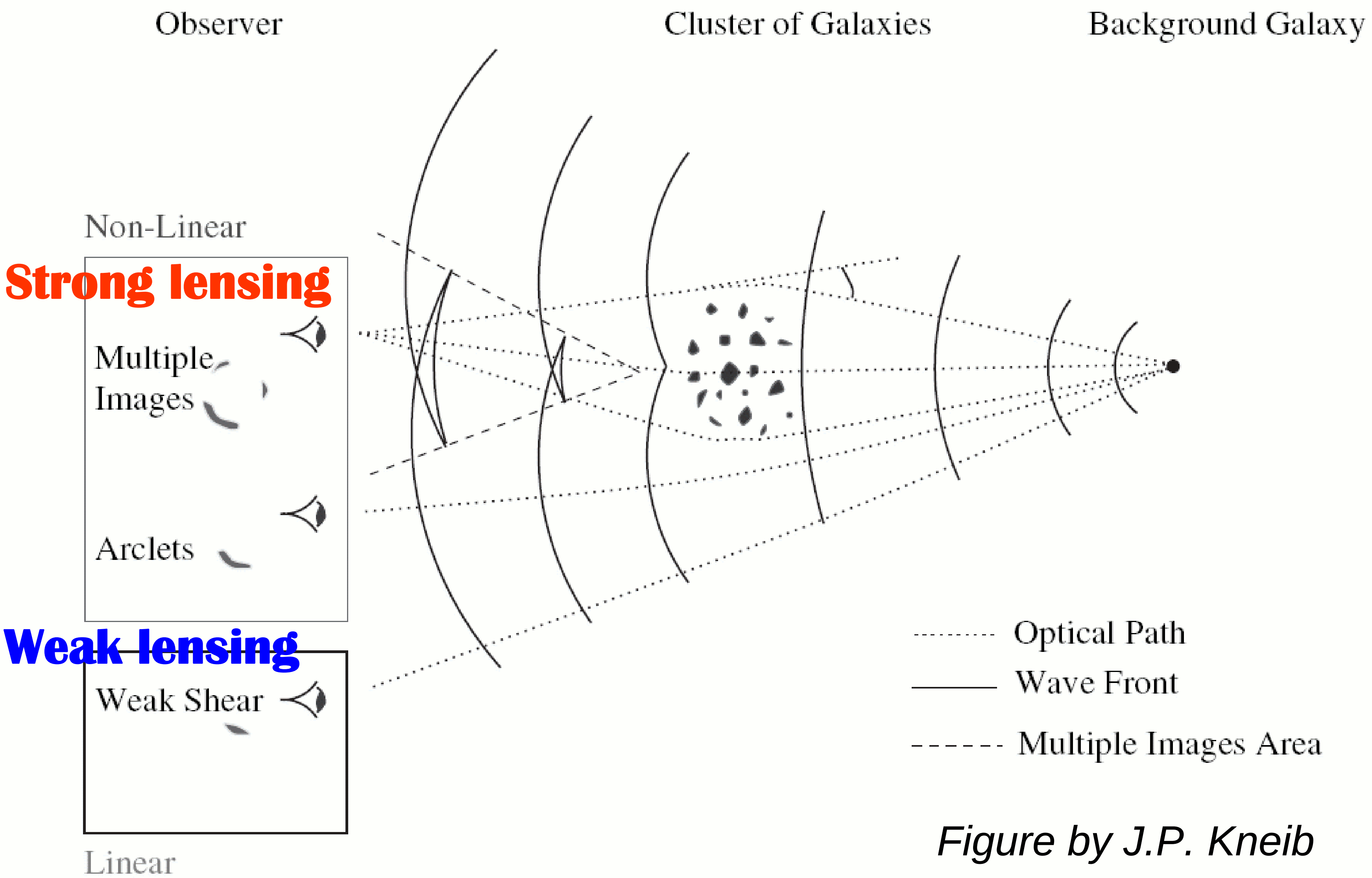

Figure by J.P. Kneib

Strong Lensing: Multiple Imaging

A source galaxy at z=1.675 has been multiply lensed into 5 apparent images

CL0024+1654 (z=0.395)

HST/WFPC2

Strong Lensing: Arcs, arcs, arcs!

A1689 (z=0.183): One of the most massive clusters known. A total of >100 multiply-lensed images of ~30 background galaxies identified by SL modeling

Strong Lensing: Giant Luminous Arcs

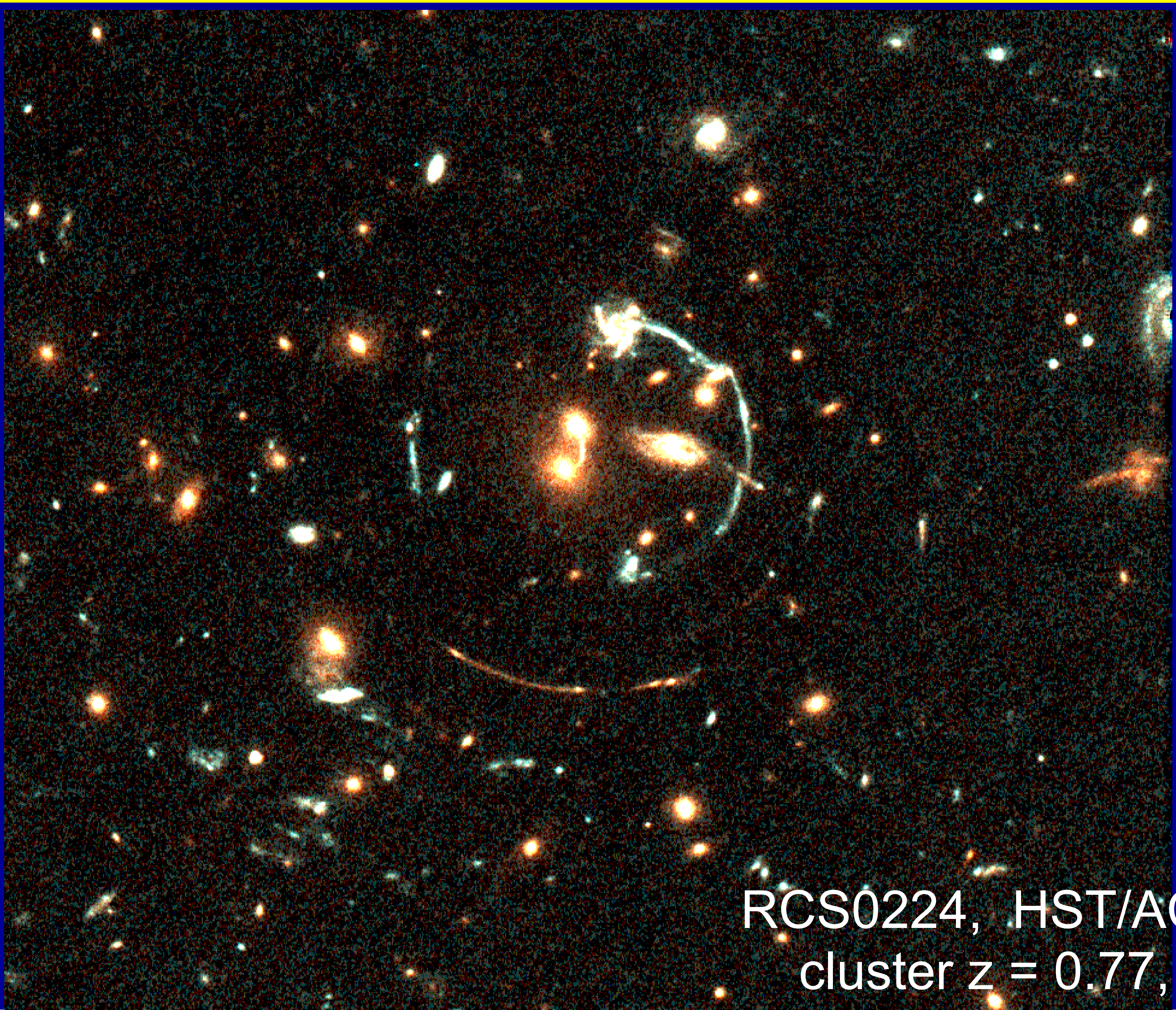

RCS0224, HST/ACS
cluster z = 0.77, arc z = 4.89

Weak Gravitational Lensing (WL)

Cluster z = 0.77; Arc z = 4.89: Photo from H. Yee (HST/ACS)

Observable tangential alignment of background galaxy images, probing the underlying gravitational field of cosmic structure

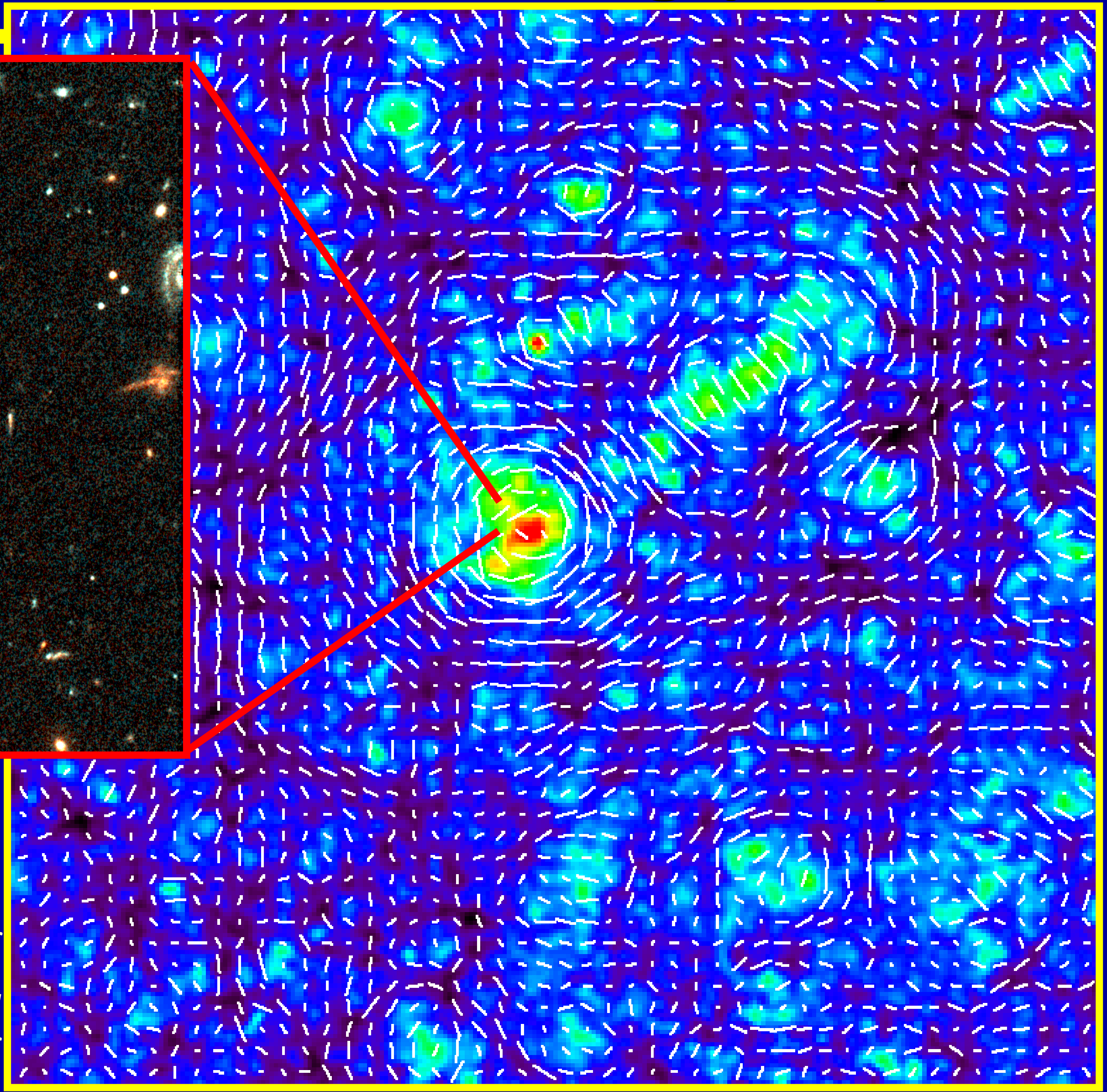

Simulated 3x3 degree field (Hamana 02)

Quadrupole Weak Lensing

Differential deflection causes a distortion in "**area**" and "**shape**" of an image

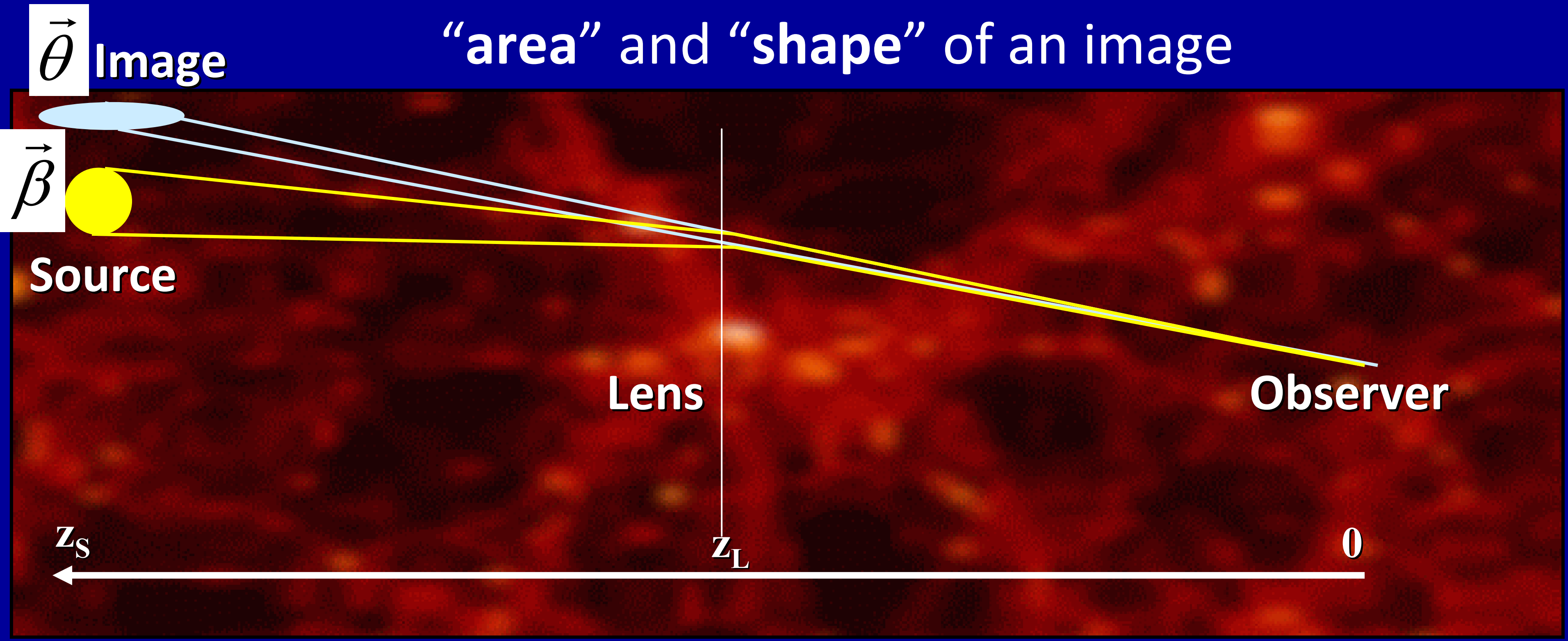

Deformation of shape/area of an image

$$\delta\beta_i = \mathbf{A}_{ij}\delta\theta_j + O(\delta\theta^2)$$

For an infinitesimal source:

$$d^2\vec{\beta} = \mathbf{A}\, d^2\vec{\theta}$$

A: Jacobian matrix of the lens equation

Effects of Convergence and Shear

Local lens mapping by Jacobian matrix, A_{ij}

$$\mathbf{A}_{ij}(\boldsymbol{\theta}) = \delta_{ij} - \psi_{ij}$$

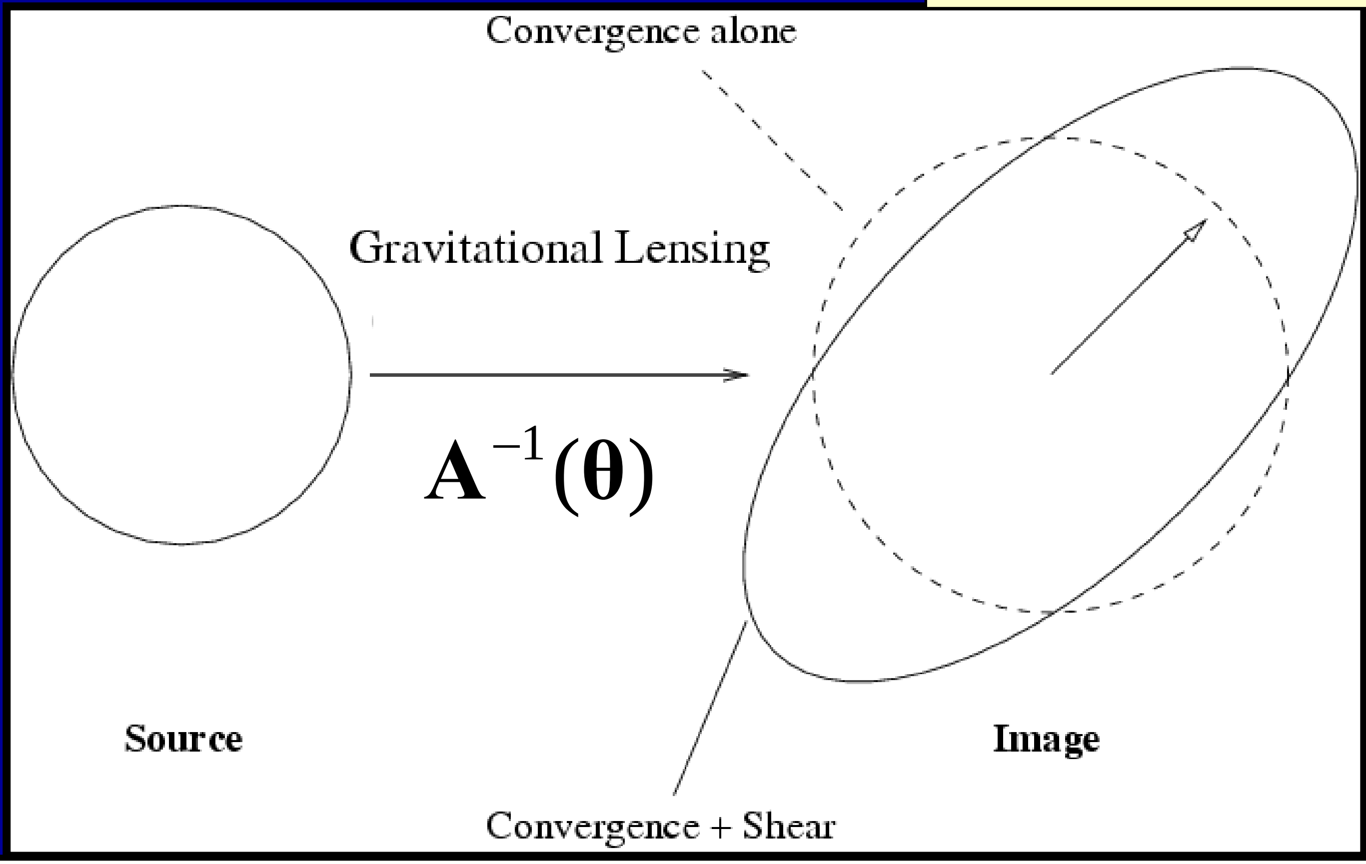

$$\mathcal{A}(\boldsymbol{\theta}) = \begin{pmatrix} 1-\kappa-\gamma_1 & -\gamma_2 \\ -\gamma_2 & 1-\kappa+\gamma_1 \end{pmatrix} = (1-\kappa)\begin{pmatrix} 1 & 0 \\ 0 & 1 \end{pmatrix} - \begin{pmatrix} \gamma_1 & \gamma_2 \\ \gamma_2 & -\gamma_1 \end{pmatrix},$$

Physical Meaning of κ

Lensing Convergence: weighted-projection of mass overdensity

$$\kappa(\boldsymbol{\theta}) \equiv \frac{1}{2}\Delta^{(2)}\psi(\boldsymbol{\theta}) = \int dl\, \delta\rho_m \left(\frac{c^2}{4\pi G} \frac{D_{OS}}{D_{OL} D_{LS}} \right)^{-1} \approx \frac{\Sigma_m(\boldsymbol{\theta})}{\Sigma_{\rm crit}}$$

Critical surface mass density of gravitational lensing

$$\Sigma_{\rm crit}(z_L, z_S; \underline{\Omega_m, \Omega_\Lambda, H_0}) = \frac{c^2}{4\pi G} \frac{D_{OS}}{D_{OL} D_{LS}}$$

Strong lensing κ~1 @ high density regions (r<~100kpc/h)

probability

Weak lensing κ~0.1 @ r ~[100-2000]kpc/h

Cosmic shear κ~0.01 @ Large Scale Structure (~10Mpc)

Note, this is only a crude definition, as lensing also depends on the (trace-free) tidal shear field.

E and B Mode Gravitational Distortions

Shear matrix with 2 degrees-of-freedom can be expressed with 2 scalar potentials (e.g., Crittenden et al. 2002):

Shear matrix in terms of potential:

$$\Gamma_{ij} = \left(\partial_i \partial_j - \frac{1}{2}\delta_{ij}\Delta \right)\psi_E + \frac{1}{2}\left(\varepsilon_{kj}\partial_i\partial_k + \varepsilon_{ki}\partial_j\partial_k\right)\psi_B$$

$$\psi_E = \psi \text{ (lens potential)}$$
$$\psi_B = 0$$

In pure WL, B-mode = 0 (E>>B)

→ WL produces a tangential (E-mode) distortion pattern around the positive mass overdensity.

→ B-mode "signal" can be used to monitor residual systematics in WL measurements: e.g., PSF anisotropy

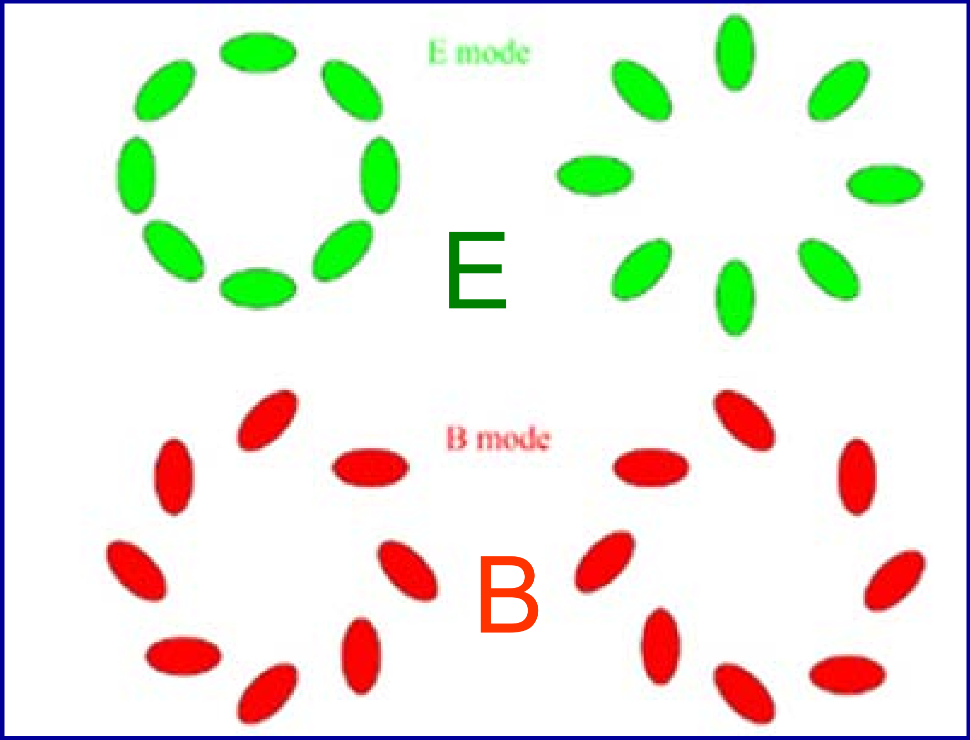

3. Cluster Lensing Effects

① Tangential Gravitational Shear

② Einstein Radius Constraint

③ Magnification Bias

(1) Weak Lensing Tangential Distortion

$$\gamma_+(r) \propto \Delta\Sigma_m(r) \equiv \overline{\Sigma}_m(<r) - \Sigma_m(r)$$

Measure of tangential coherence of distortions around the cluster (Tyson & Fisher 1990)

Mean tangential ellipticity of BG galaxies (g_+) as a function of cluster radius; uses typically (1-2) x 10^4 background galaxies per cluster, yielding typically S/N=5-15 per cluster.

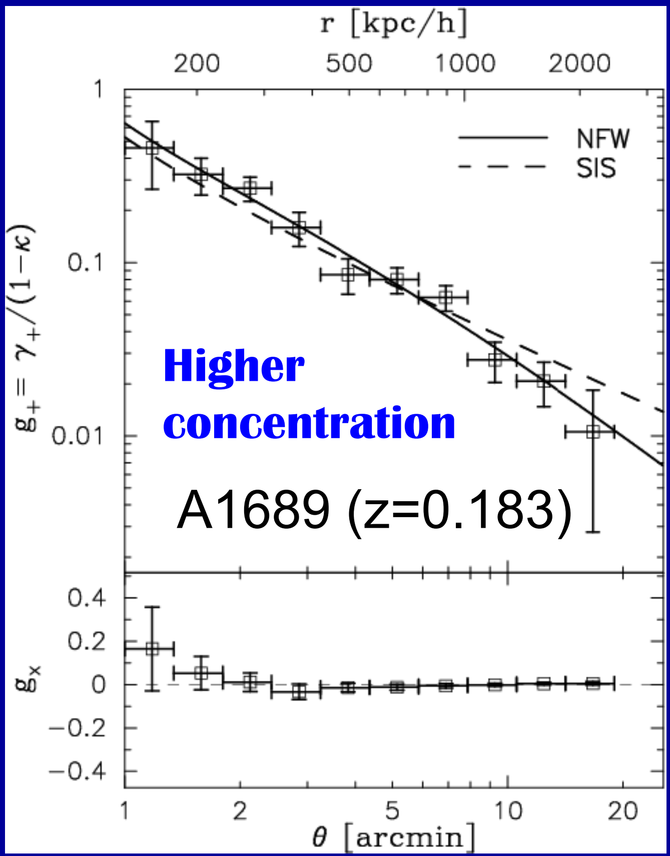

Umetsu & Broadhurst 2008, ApJ, 684 , 177

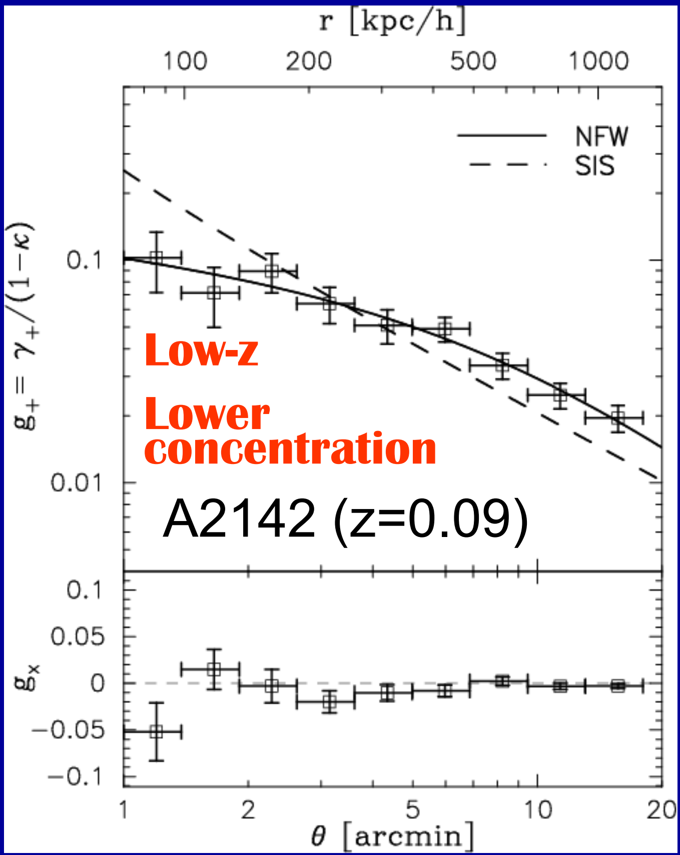

Umetsu et al 2009, ApJ, 694, 1643

(2) Einstein Radius Constraint

Lensing geometry for an Einstein ring

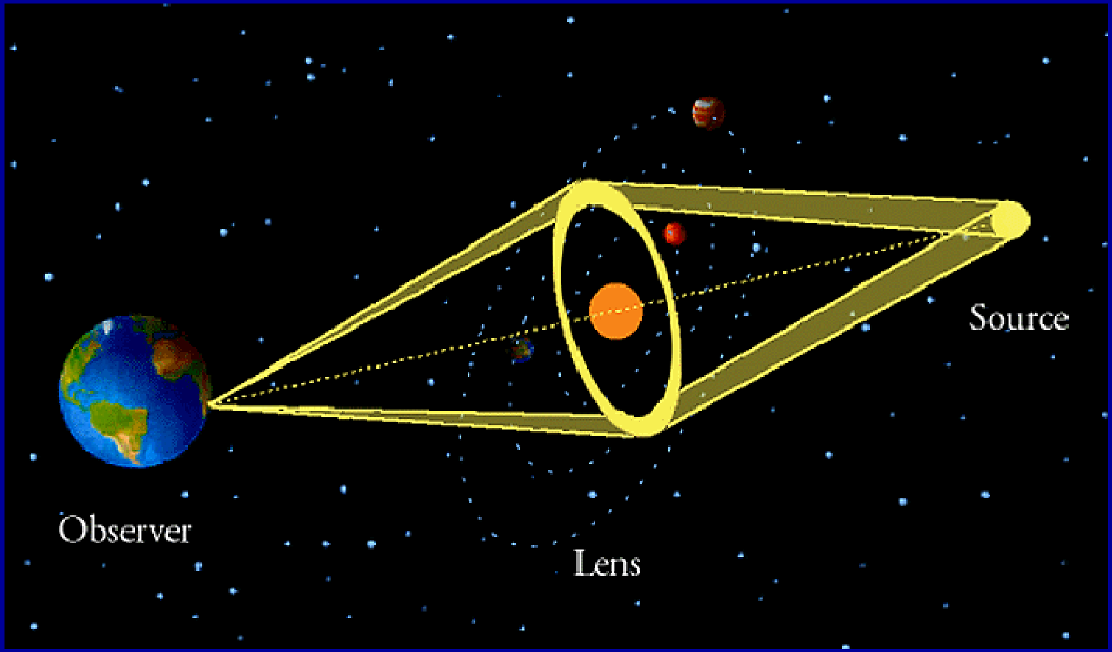

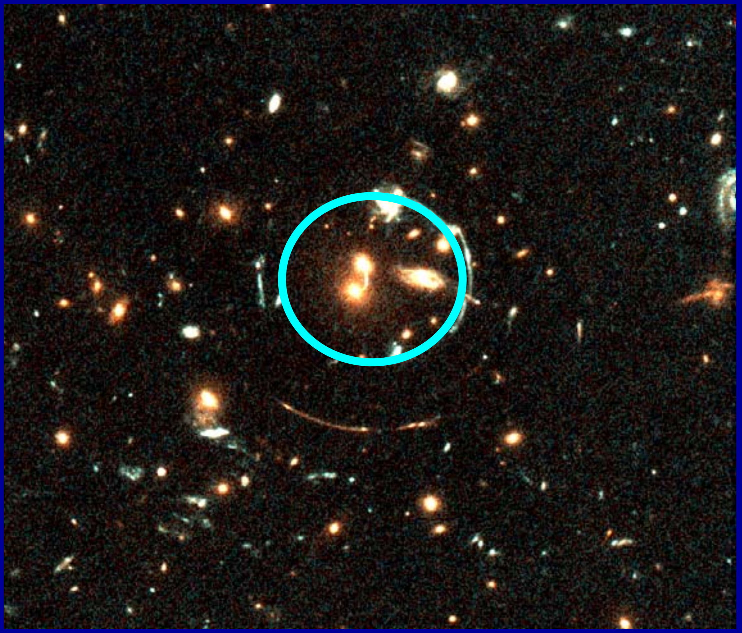

The apparent size of an Einstein ring yields a tight constraint on the interior projected mass enclosed by the arcs:

$$\theta_E = \sqrt{\frac{4GM_{\rm 2D}(<\theta_E)}{c^2}\frac{D_{LS}}{D_{OL}D_{OS}}}$$

or

$$\overline{\Sigma}_{\rm m}(<\theta_E) = \frac{c^2}{4\pi G}\frac{D_{OS}}{D_{OL}D_{LS}},$$

$$i.e., \overline{\kappa}(<\theta_E) = 1, \text{ or } {\rm g}_+(\theta_E) = 1$$

WL Tangential Distortion + Einstein Radius

Tangential distortion + θ_E constraint in CL0024+1654 (z=0.395)

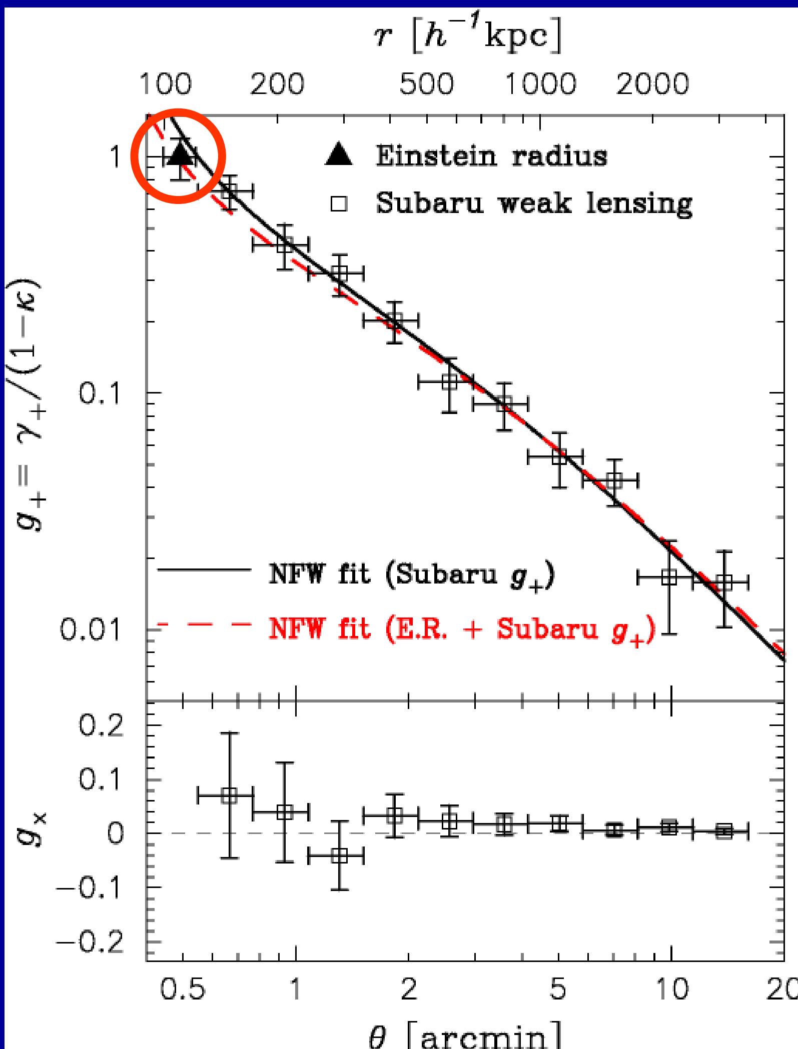

Constraints on DM Structure Parameters

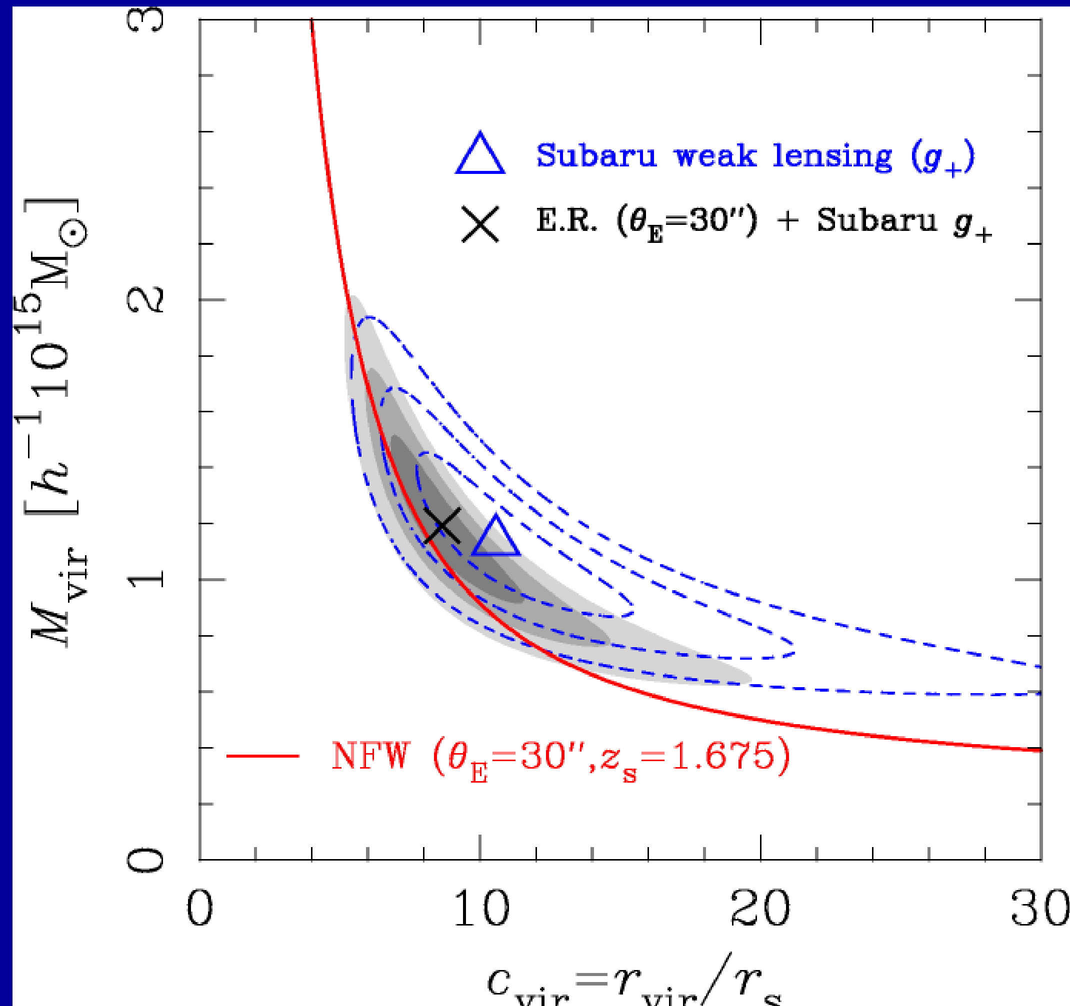

Umetsu et al. 2010, ApJ in press, arXiv:0908.0069

(3) Weak Lensing Magnification Bias

Magnification bias: Lensing-induced fluctuations in the background density field (Broadhurst, Taylor, & Peacock 1995)

$$\delta n(\boldsymbol{\theta}) / n_0 \approx -2(1 - 2.5\alpha)\kappa(\boldsymbol{\theta})$$

with unlensed counts of background galaxies $n_0(< m) \propto 10^{\alpha m}$

When the count-slope is <0.4 (=lens invariant slope), a net deficit is expected.

Example of Magnification Bias Measurement

Count depletion of "red" galaxies in CL0024+1654 (z=0.395)

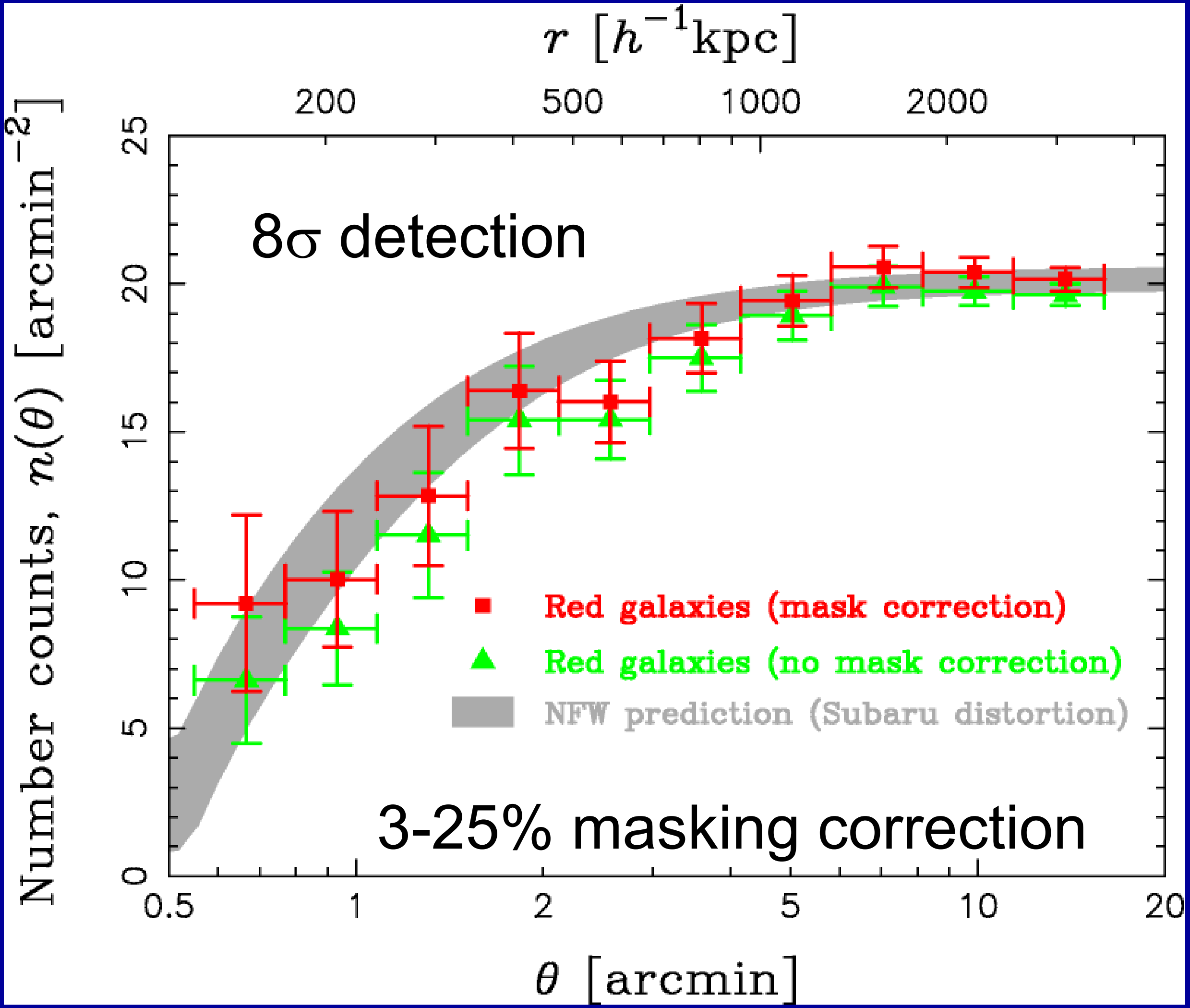

Distortion of "blue+red" sample

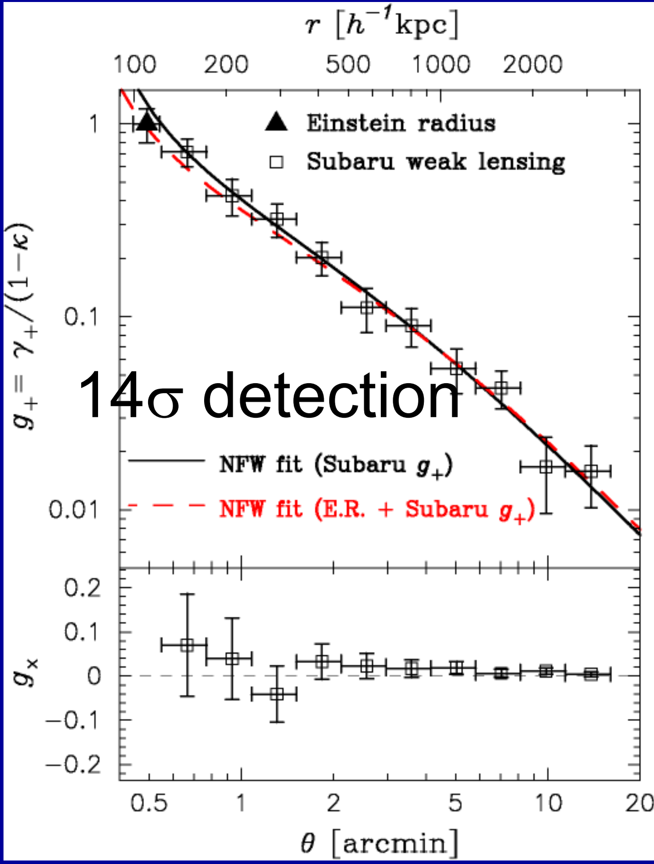

Umetsu et al. 2010, ApJ in press, arXiv:0908.0069

4. Highlights of Cluster Lensing Constraints on the DM Halo Density Profiles

[1] Full Weak + Strong Lensing Analysis

Combining WL (~10^4 weakly lensed images) and SL (~30-100 strongly lensed images)

→ Probing the mass density profile from 10kpc/h to 2000kpc/h

Results for Abell 1689 (z=0.183) and CL0024+1654 (z=0.395)

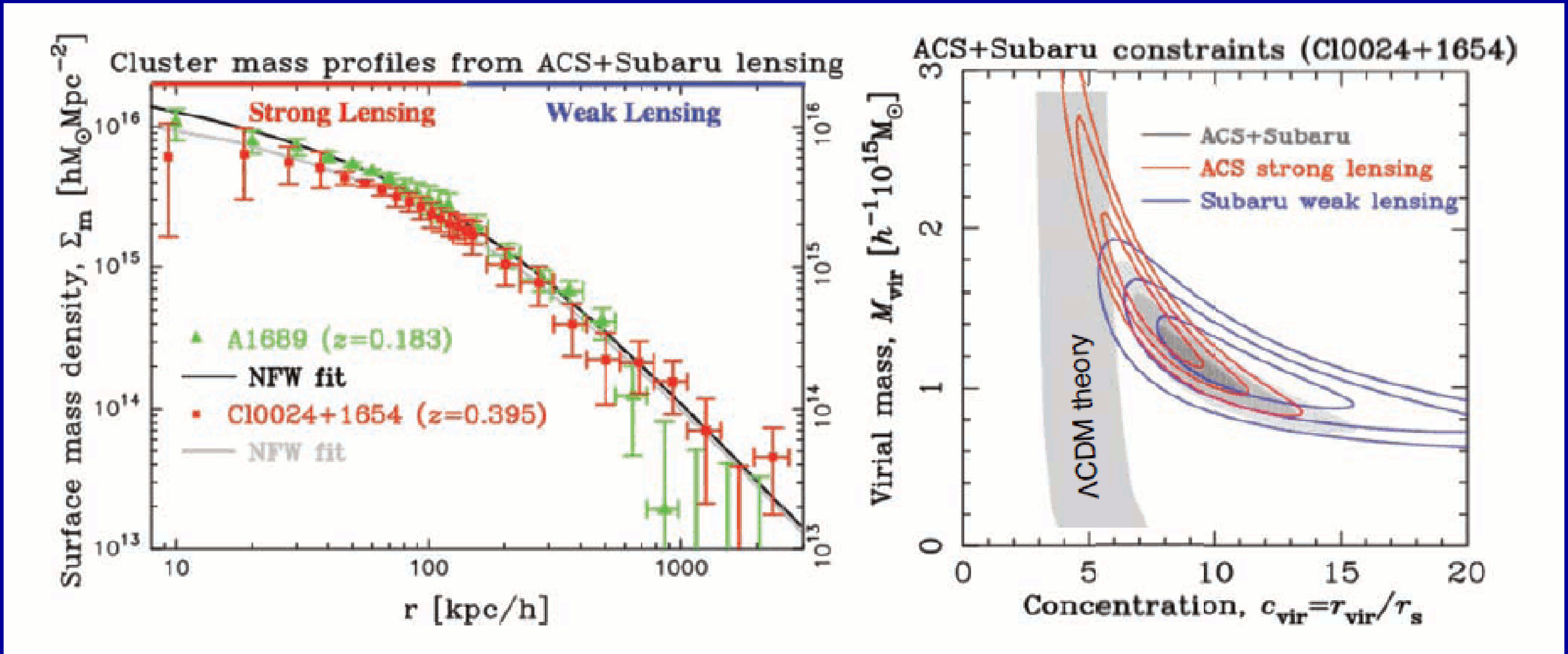

The profile shapes are consistent with CDM (NFW) over the entire cluster, but the degree of concentration is much higher than expected for LCDM.

Umetsu & Broadhurst 2008, ApJ, 684, 177 (A1689)

Umetsu et al. 2010, ApJ in press, arXiv:0908.0069 (CL0024+1654)

Lensing Constraints on the Central Cusp Slope

Weak + strong lensing constraints on CL0024+1654 (z=0.395)

Generalized NFW (gNFW) profile w/ 3 free parameters:

$$\rho(r)/\rho_s = \frac{1}{(r/r_s)^{\alpha}(1+r/r_s)^{(3-\alpha)}}$$

$$c_{-2} := \frac{r_{vir}}{(2-\alpha)r_s}$$

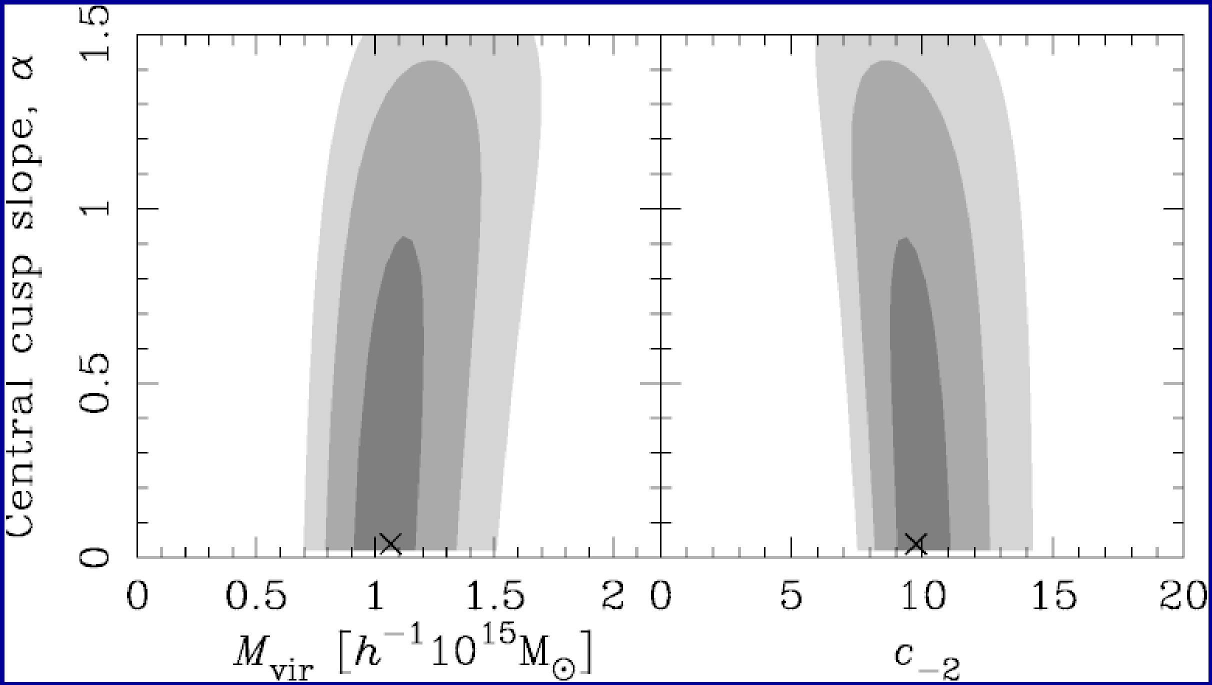

- Central cusp slope α < 1 at 68.3%CL from the combined strong and weak lensing constraints – yet consistent with NFW.
- Cored profile (α~0) is preferred (cf. Tyson et al. 1998; CDM crisis)
- Note CL0024 is the result of a line-of-sight collision of 2 similar-mass clusters, viewed approximately 2-3Gyr after impact (see Umetsu et al. 2010, ApJ in press)

[2] Testing LCDM by Cluster Lensing Profiles

"WL distortion + Einstein-radius constraint" (left) vs. "WL magnification bias" (right) in 4 high-mass clusters:

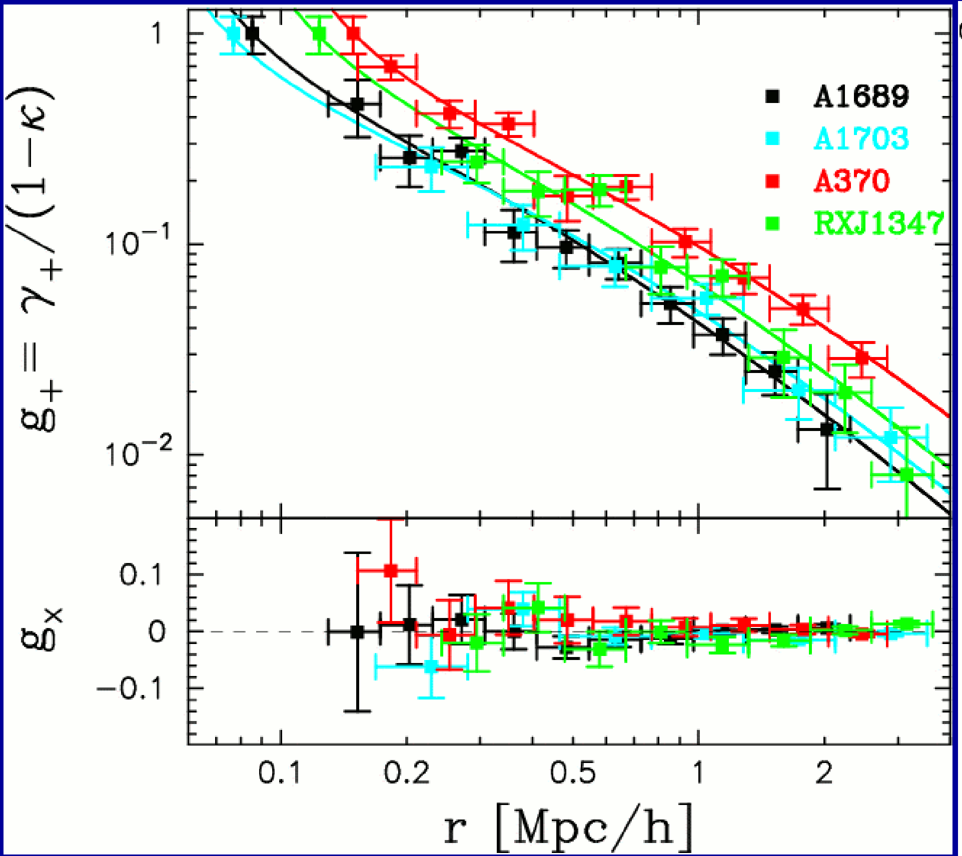

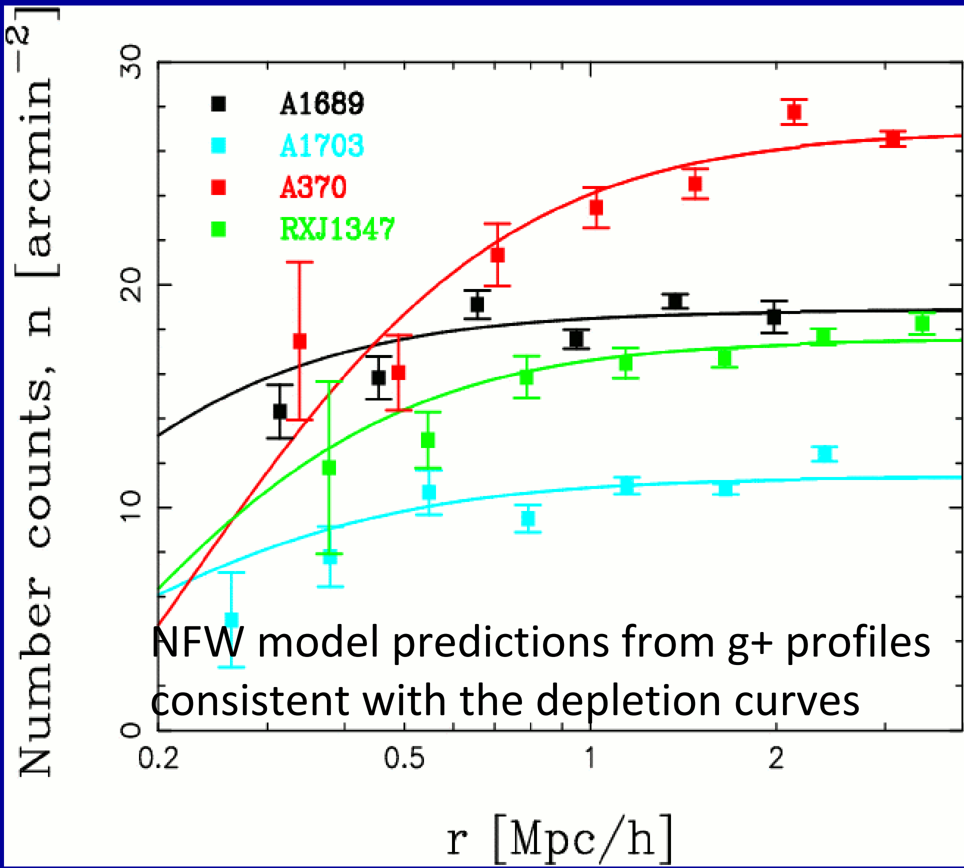

Observed curves are similar in form, well described by CDM-consistent NFW profiles

Broadhurst, Umetsu, Medezinski+ 2008, ApJ, 685, L9

First Lensing Test of the C-M Relation

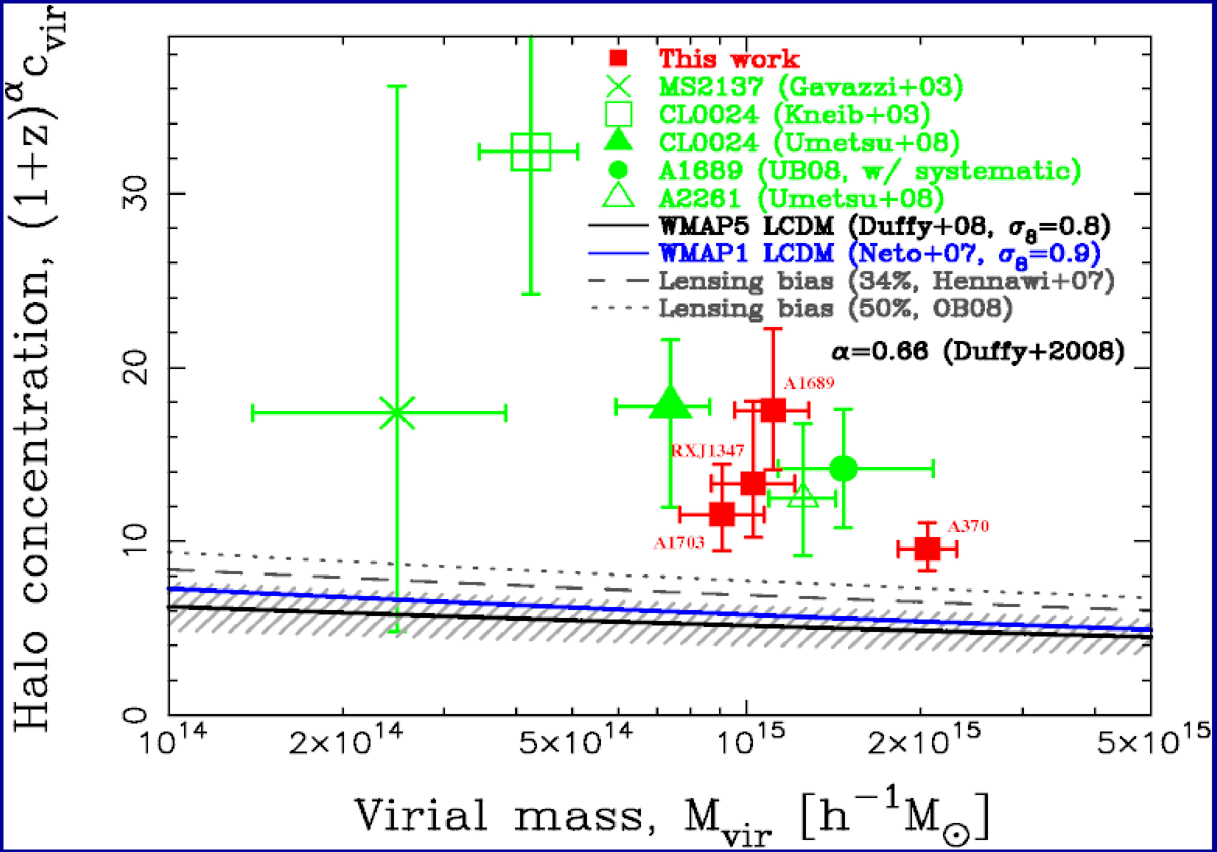

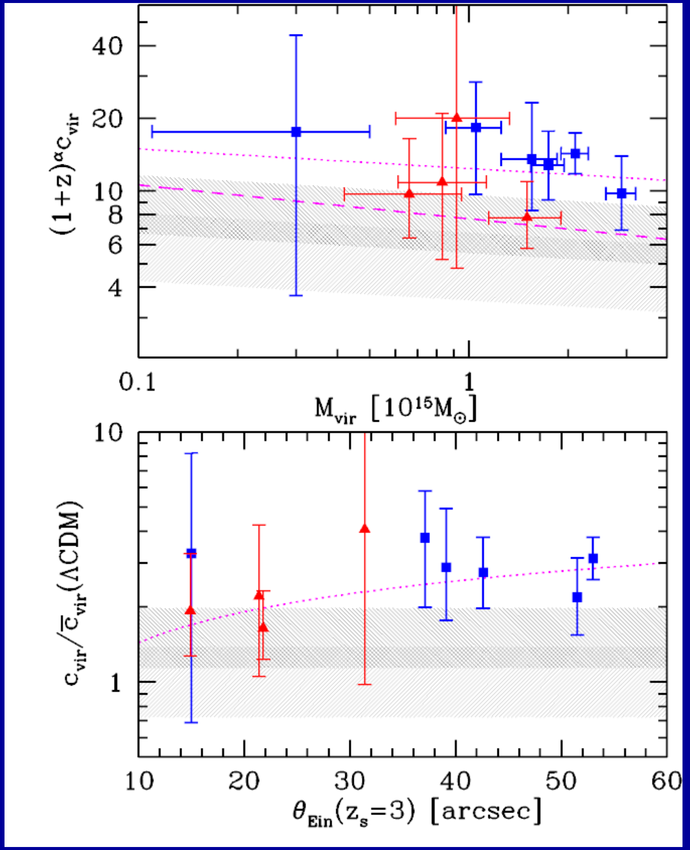

Taking into account an orientation bias correction of **+18%,** discrepancy is still 4σ.
With a **50% bias** correction, it represents a 3σ deviation (BUM+2008)

Left) Broadhurst, Umetsu, Medezinski+ 2008, ApJ, 685, L9 (BUM+2008)

Right) Oguri et al. 2009, ApJ, 699, 1038

Results and Implications?

Results:

- BUM+2008: $<C_{vir}>=10\pm1$ for $<M_{vir}>=1.25\times10^{15}\ M_{sun}/h$
- Oguri+2009: $<C_{vir}>\sim8$; larger the θ_E, higher the concentration
- Both found a significant **over-concentration** w.r.t. LCDM, $<C_{vir}>=5\pm1$, even after correcting for the selection/orientation bias (+50% at most)

→Clusters formed earlier (z>~1) than expected (z<~0.5)?

Possible Solutions:

— Accelerated growth factors of density perturbation for a generalized DE Equation-of-State (e.g., Sadeh & Rephaeli 2008)

— Non Gaussianity in the primordial density perturbation to advance cluster formation (e.g., Matthis, Diego, & Silk 2004)

Nevertheless, detailed SL modeling (i.e., HST data!!) is needed for accurate determination of halo concentration, and hence for a stringent test of LCDM

[3] Stacked Cluster Weak Lensing Analysis

Stacking WL distortion profiles of an "unbiased" sample of clusters

→ less sensitive to substructures/asphericity of individual clusters

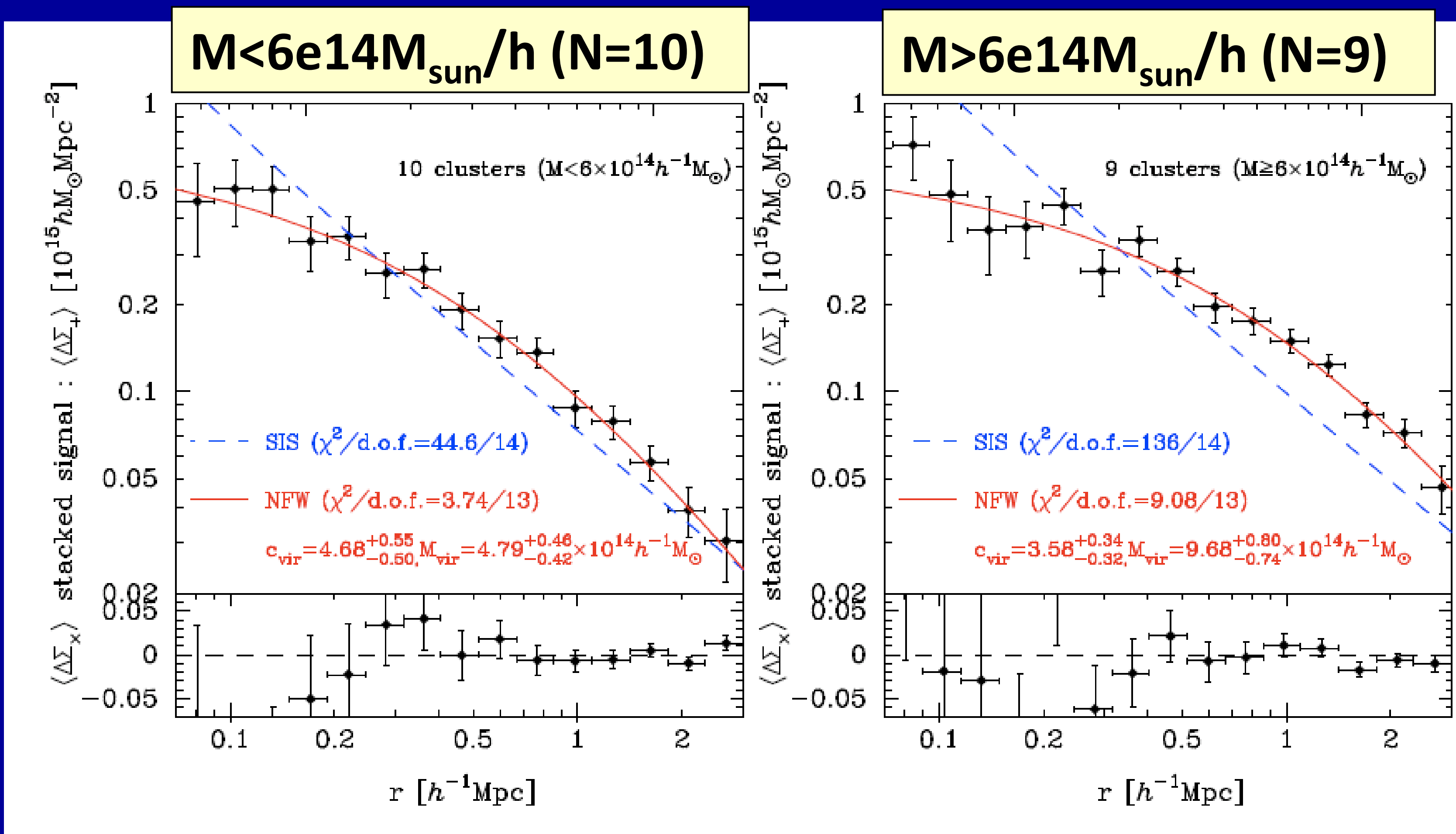

SIS rejected @6 and 11 σ levels (Okabe,Takada,Umetsu+ 10, arXiv:0903.1103)

C-M Relation: Observations vs. Theory

Subaru WL (19 clusters)

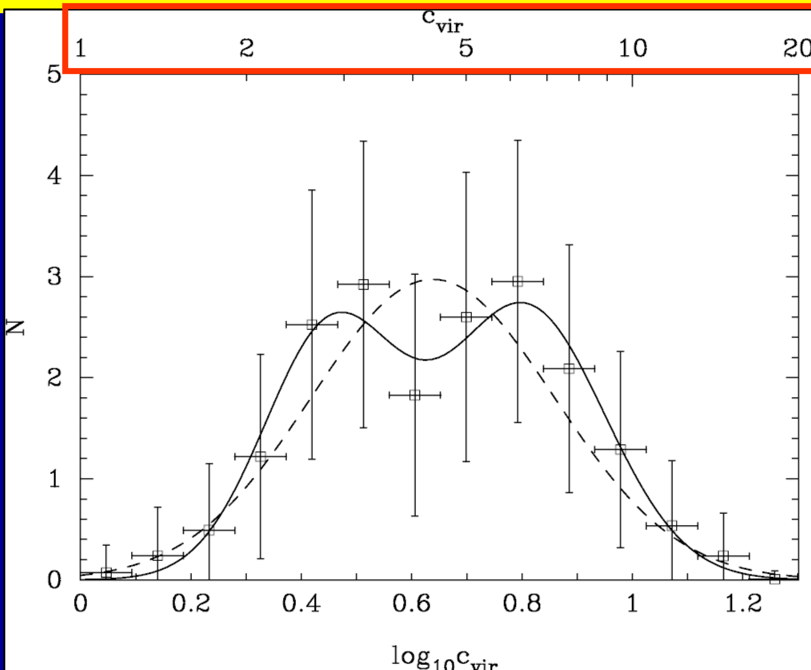

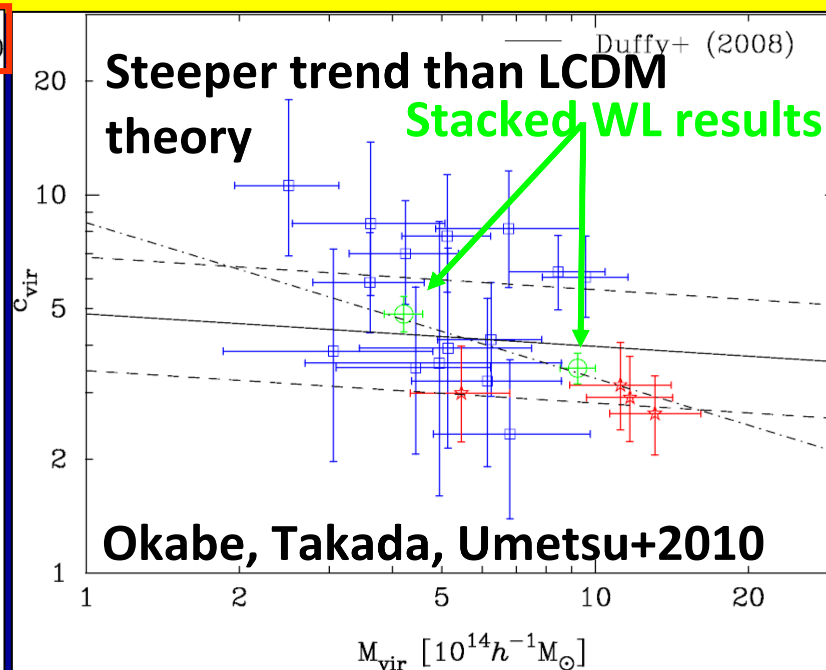

LCDM theory

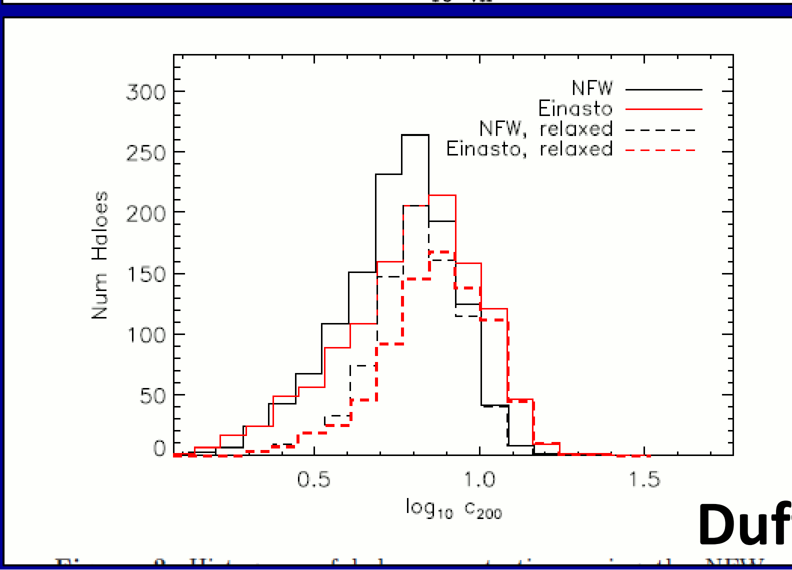

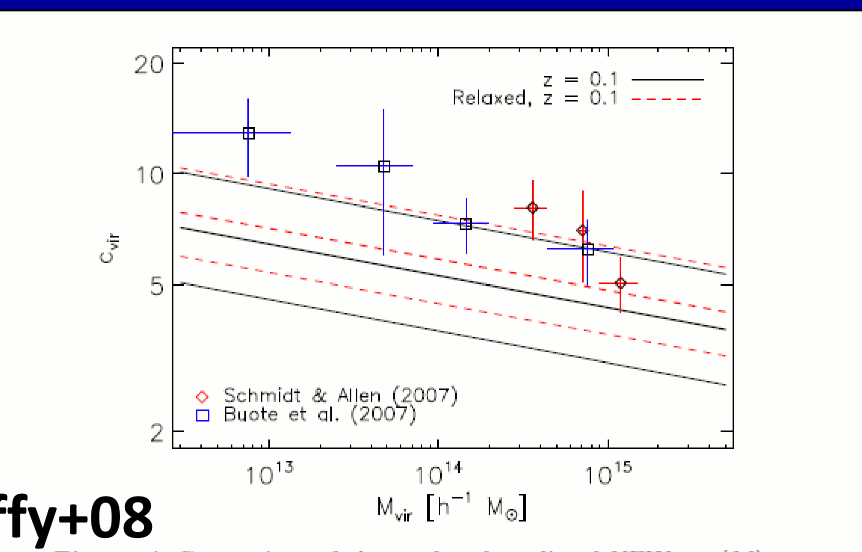

Duffy+08

Summary

- To date, detailed full mass profiles $\Sigma_m(r)$ have been measured for several clusters (A1689, CL0024, A1703 by our group) from joint weak + strong lensing analysis, and show a continuously steepening radial trend, consistent with the collisionless CDM model.
- Such a joint measurement is so far limited by the availability of deep, high-resolution space-telescope (HST/ACS) data.
- The exact cusp (1-1.5?) and outer (3-4?) slopes are yet to be determined from a larger sample of clusters.
- Massive clusters with strong-lensing based Einstein-radius measurements (N~10 so far) show higher-than-expected mass concentrations, indicating a tension with the standard LCDM model.
- Statistical stacked weak lensing analysis is very promising and complementary to joint strong+weak lensing analysis, but is yet insensitive to the inner profile. This results in a (noise-induced) correlation between (M_{vir}, C_{vir}).

5. Future Work

CLASH:

Cluster Lensing And Supernova survey with Hubble

An HST Multi-Cycle Treasury Program designed to place new constraints on the fundamental components of the cosmos: dark matter, dark energy, and baryons.

WFC3 (UVIS + IR) and ACS will be used to image 25 relaxed clusters in 14 passbands from 0.22 - 1.6 microns. Total exposure time per cluster: 20 orbits.

Clusters chosen based on their smooth and symmetric x-ray surface brightness profiles. Minimizes lensing bias. All clusters have $T > 5$ keV with masses ranging from ~5 to ~30 x $10^{14} M_{\odot}$. Redshift range covered: $0.18 < z < 0.90$.

Multiple epochs enable a $z > 1$ SN search in the surrounding field (where lensing magnification is low).

Marc Postman (P.I.)	Megan Donahue	Dani Maoz	Stella Seitz
Matthias Bartelmann	Rosa Gonzales-Delgado	Elinor Medezinski	Keiichi Umetsu
Narciso Benitez	Holland Ford	Leonidas Moustakas	Arjen van der Wel
Larry Bradley	Leopoldo Infante	Eniko Regoes	Wei Zheng
Tom Broadhurst	Daniel Kelson	Adam Riess	Adi Zitrin
Dan Coe	Ofer Lahav	Piero Rosati	

CLASH: An HST Multi-Cycle Treasury Program

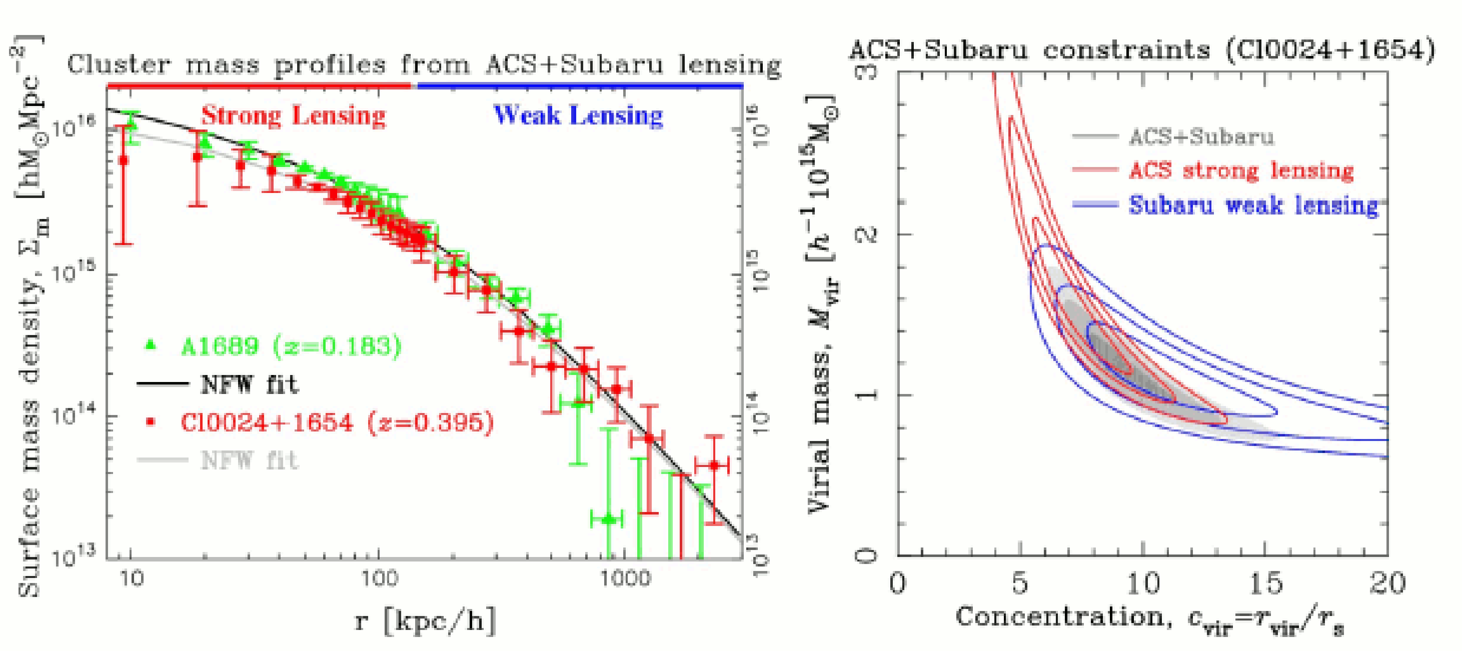

Both strong AND weak lensing measurements are needed to make accurate constraints on the DM profile.

CLASH data will allow us to definitively derive the representative equilibrium mass profile shape and robustly measure the cluster DM mass concentrations and their dispersion as a function of cluster mass *and their evolution with redshift.*

CLASH: An HST Multi-Cycle Treasury Program

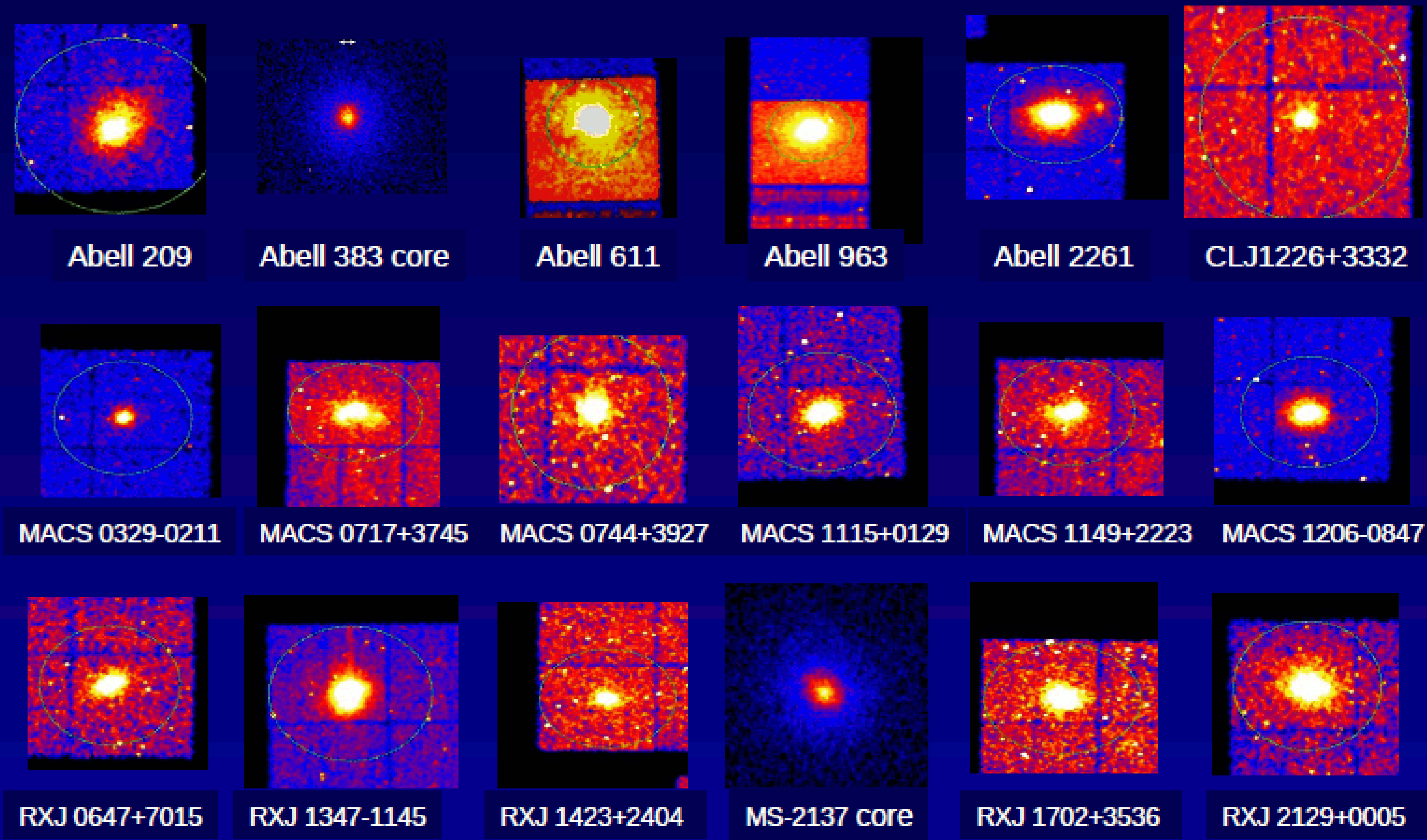

Cutouts of Chandra images of 18 of the 25 CLASH clusters from ACCESS database

CLASH: An HST Multi-Cycle Treasury Program

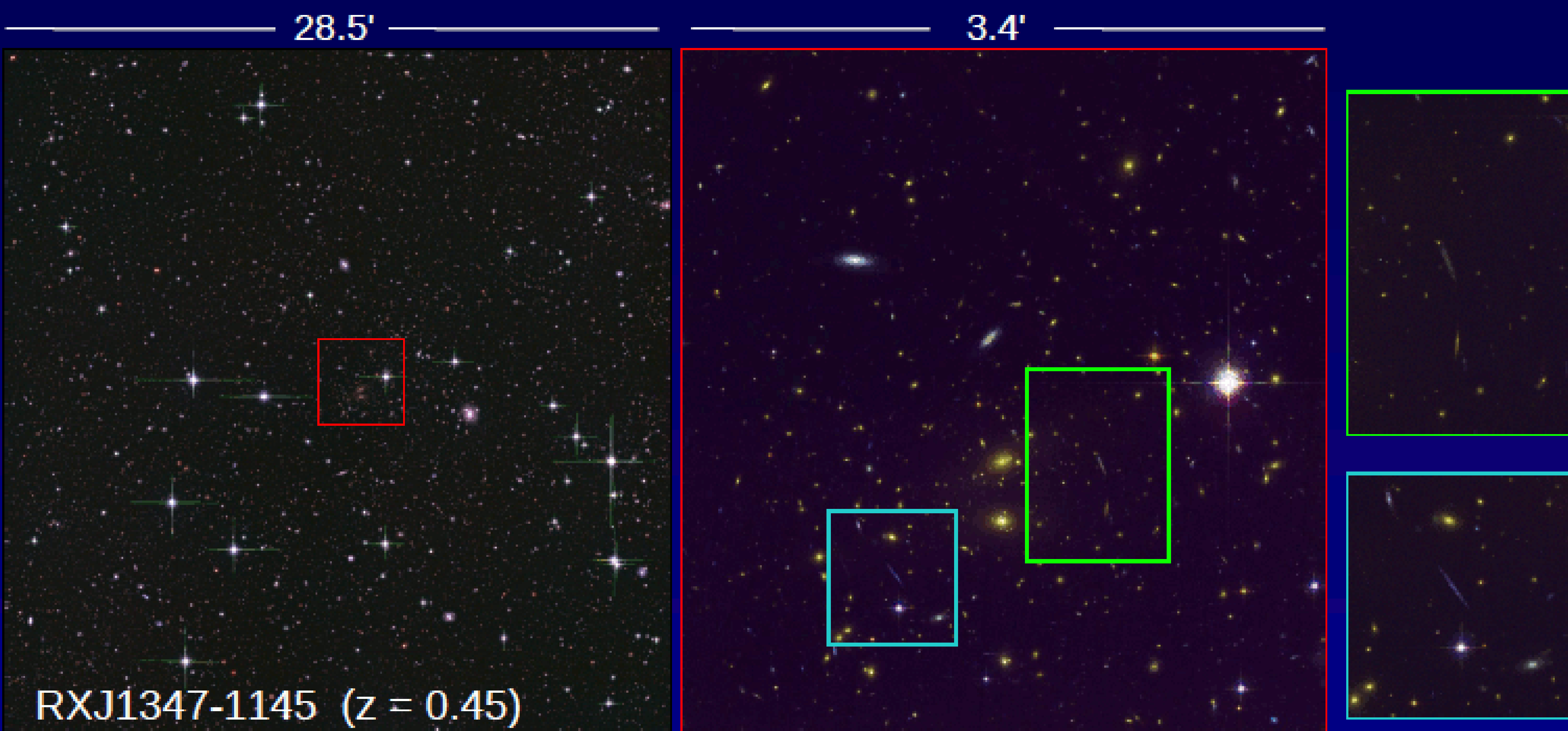

SUPRIME CAM Image ACS/WFC Image

CLASH: An HST Multi-Cycle Treasury Program

Why 14 filters?

Will yield photometric redshifts with rms error of ~2% x (1 + z) for sources down to ~26 AB mag.

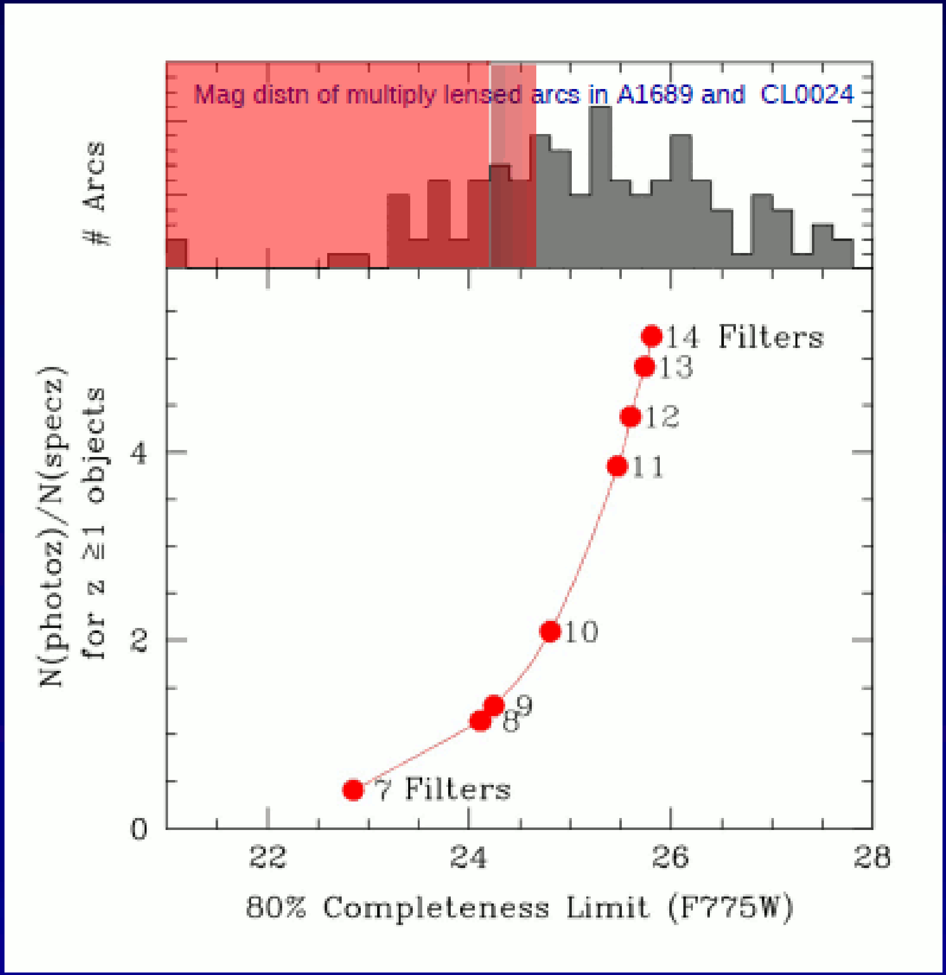

With 14 filters, 80% photo-z completeness is reached at AB ~26 mag and useful redshift information is available for ~5 times as many lensed objects than would be possible solely from spectroscopically acquired redshifts.

CLASH: An HST Multi-Cycle Treasury Program

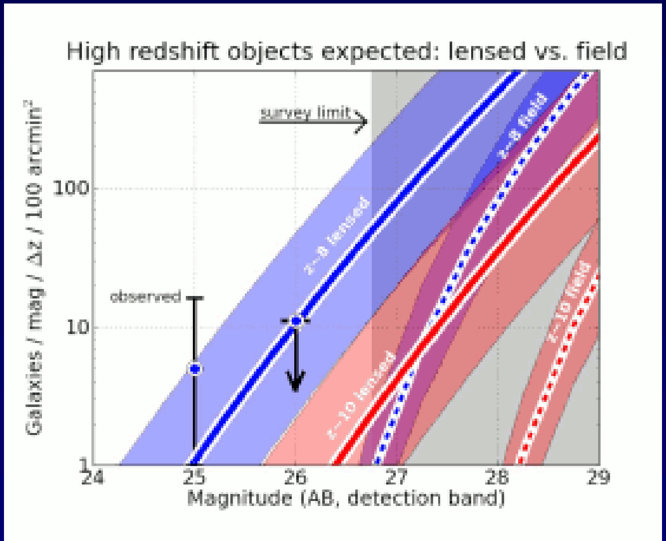

The blue and red solid curves show the expected number of z=8 and z=10 galaxies, respectively, to be discovered behind our 25 clusters as a function of magnitude in the detection band (F110W at z=8 and F140W at z=10).

A significant advantage of searching for high-z objects behind strongly lensing clusters is that the lens model can also be used to discriminate between highly-reddened objects and truly distant, high-z objects as the projected position of the lensed image is a strong function of the source redshift.

The parallel fields of the cluster survey provide the means to find ~10 SNe Ia at z >1 and *would double the number of known SNe Ia at z* > 1.2 (and potentially more, the precise number depending on the assumed time delay).

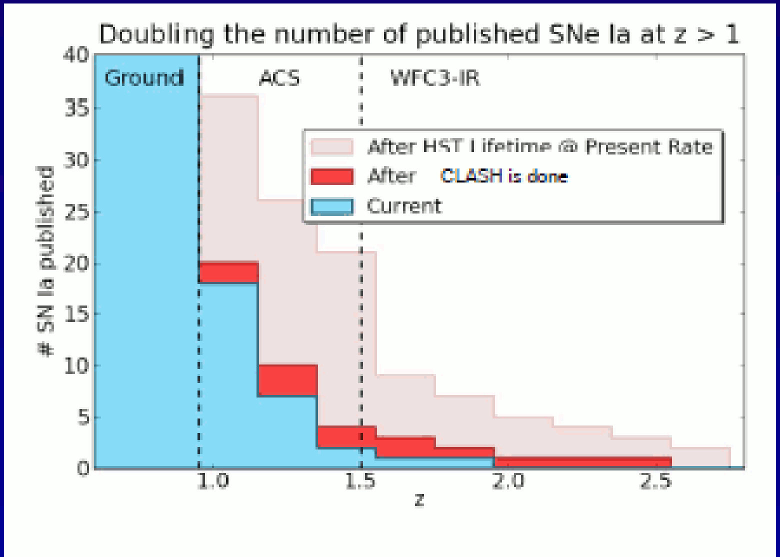

CLASH: An HST Multi-Cycle Treasury Program

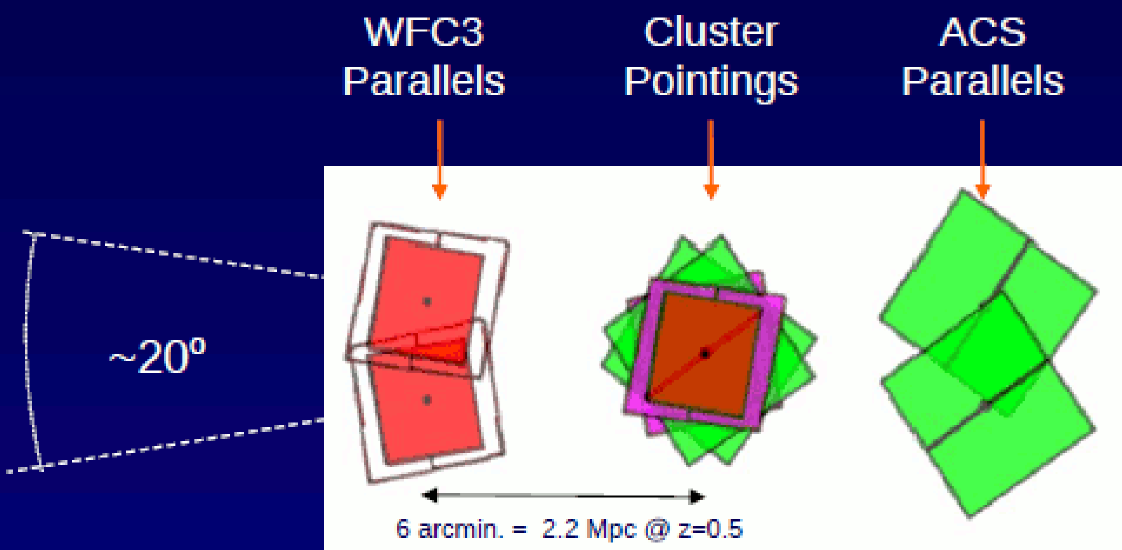

Footprint of our 2 ORIENT survey. ACS FOV in green, WFC3/IR FOV in red, WFC3/UVIS in magenta. The area of the complete 14-band coverage in the cluster center is 4.07 square arcminutes (88% of the WFC3/IR FOV).

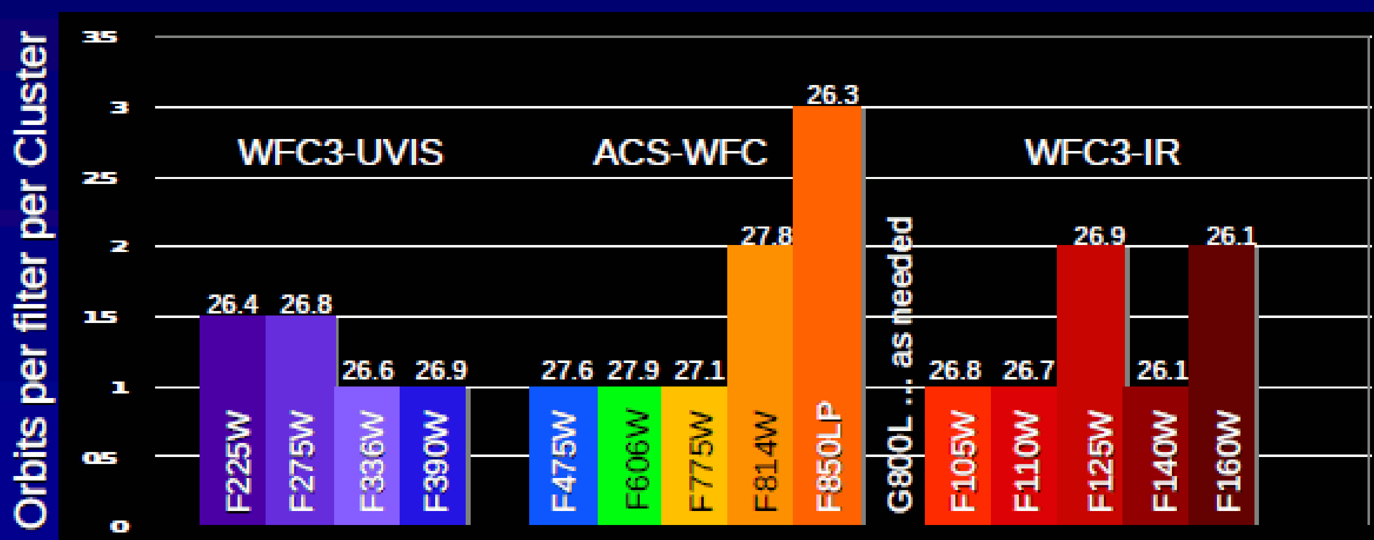

Limiting SNR=5 AB magnitudes (for flat spectrum point source) for each passband shown above

Backup Slides

Geometric Scaling of Lensing Signal

Distnace raito as a function of source z

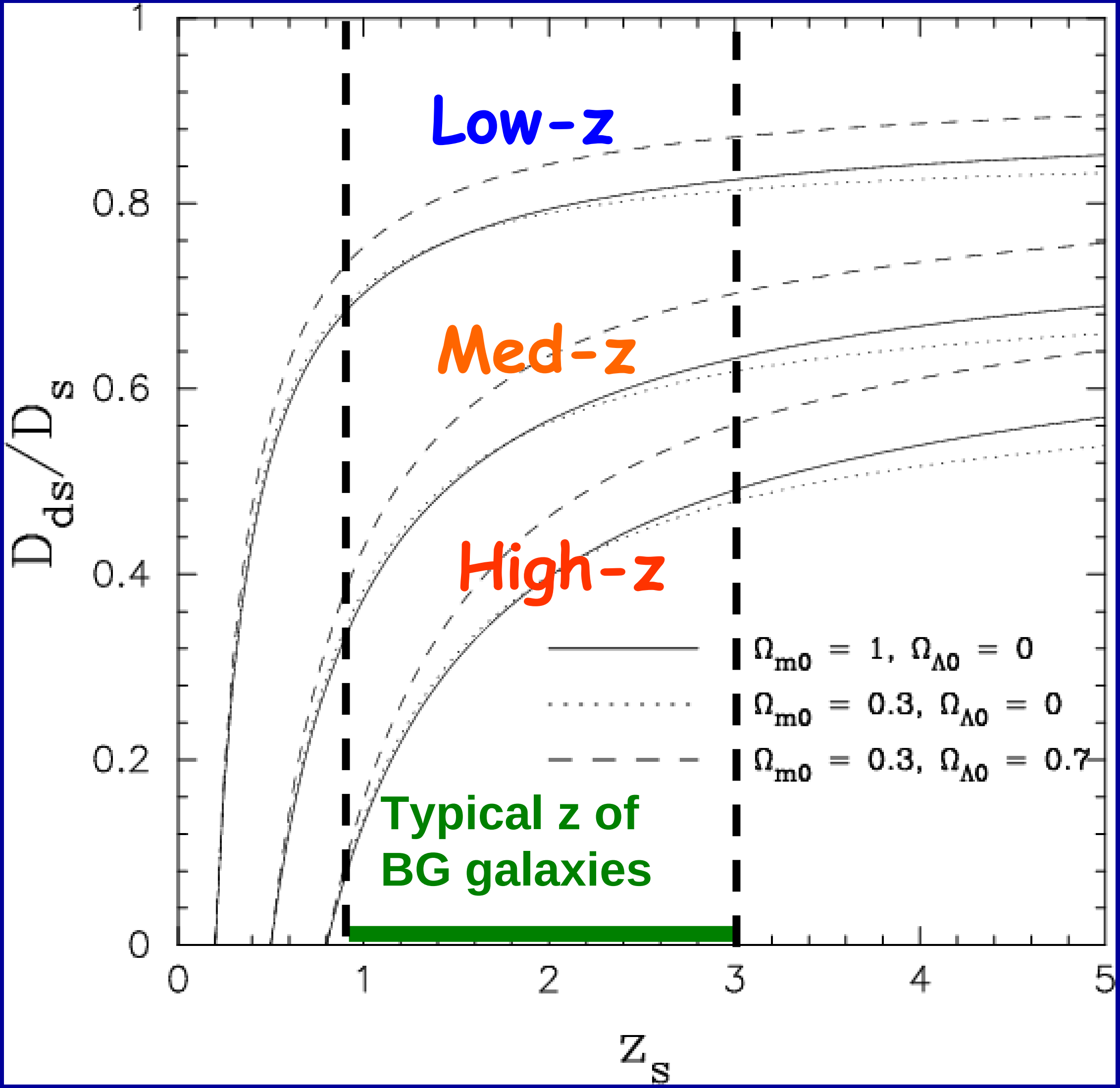

Physical mass to signal units

$$\kappa(\boldsymbol{\theta}) \propto \left(\frac{D_{ds}}{D_s}\right)\Sigma_m(\boldsymbol{\theta})$$

Low-z cluster:

zd=0.2

Med-z cluster:

zd=0.5

High-z cluster:

zd=0.8

Gravitational Shear Field

2x2 shear matrix: describes Quadrupole Shape Distortions (2 DoF)

- Coordinate dependent (cf. Stokes Q,U)
- Spin-2 “directional” quantity
- **Observable as an image ellipticity in the WL limit ($|\kappa|,|\gamma|<<1$)**

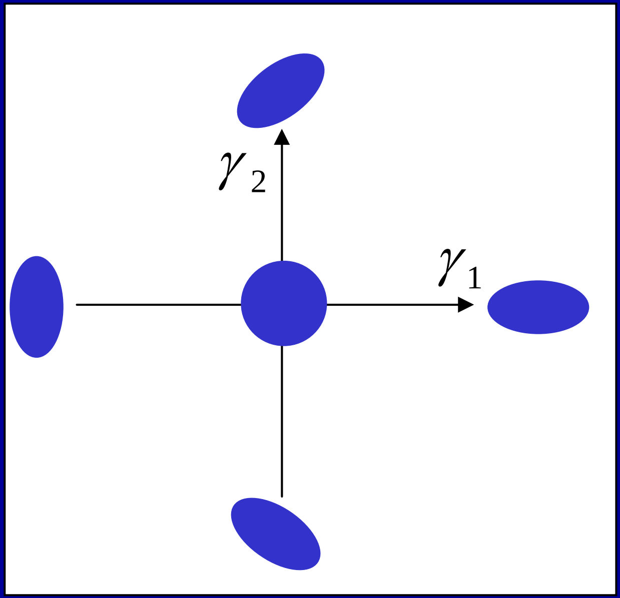

$$\Gamma_{ij} = \begin{bmatrix} +\gamma_1 & \gamma_2 \\ \gamma_2 & -\gamma_1 \end{bmatrix} \Leftrightarrow \begin{bmatrix} +Q & U \\ U & -Q \end{bmatrix}$$

Spin-2 complex shear field

$$\gamma(\boldsymbol{\theta}) = \gamma_1 + i\gamma_2 \equiv |\gamma| e^{2i\phi_\gamma}$$

Measurement of the Shear: Moment Method

Image quadrupoles:

$$Q_{ij} = \langle x_i x_j \rangle$$

Quadrupole moments of the object surface brightness

Complex ellipticity, e = e_1+ie_2:

$$e_1 = \frac{Q_{11} - Q_{22}}{Q_{11} + Q_{22}}, \; e_2 = \frac{2Q_{12}}{Q_{11} + Q_{22}}$$

In the weak limit (κ,|γ|<<1):

Mapping from intrinsic → observed ellipticity

$$e^{\mathrm{obs}} = e^{(s)} + 2\gamma + O(|\gamma|^2)$$

e(s): source intrinsic ellipticity

Assuming that background sources have random orientations:

$$\langle e^{obs} \rangle = 2\gamma + O\left(\frac{\sigma_e}{\sqrt{N}}\right) + O\left(|\gamma|^2\right)$$

(3) Weak Lensing Mass Reconstruction

Observable shear field into a 2D mass map: "non-local"

Extract E-mode from shear matrix;

$$\Delta\kappa(\boldsymbol{\theta}) = \partial^i \partial^j \Gamma_{ij}(\boldsymbol{\theta})$$

Then, invert:

$$\kappa(\boldsymbol{\theta}) = \Delta^{-1}(\boldsymbol{\theta}, \boldsymbol{\theta}') * \left(\partial^i \partial^j \Gamma_{ij}(\boldsymbol{\theta}')\right)$$

Kaiser & Squires (1993) Inversion Method:

$$\hat{\kappa}(\vec{l}) = \cos(2\phi_l)\hat{\gamma}_1(\vec{l}) + \sin(2\phi_l)\hat{\gamma}_2(\vec{l}), \quad \vec{l} \neq 0$$

Use the Green function for 2D-Poisson equation:

But l=0 mode (DC-component) is "unconstrained".

Mass-sheet degeneracy

(in the weak lensing limit)

$$\kappa(\boldsymbol{\theta}) \rightarrow \kappa(\boldsymbol{\theta}) + const.$$

Example of Mass Reconstruction

Galaxy cluster: CL0024+1654 (z=0.395)

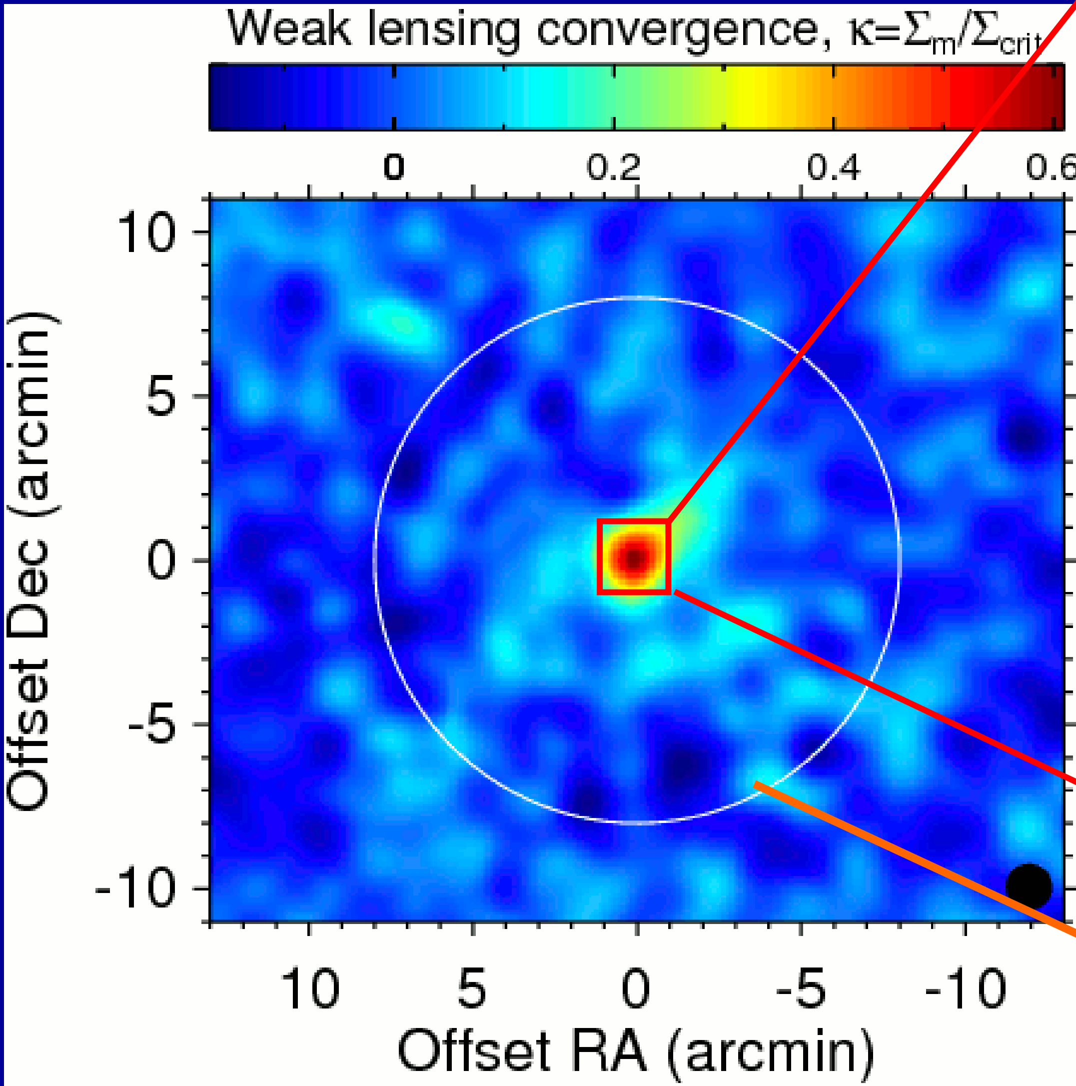

HST/ACS (3'x3' FoV)

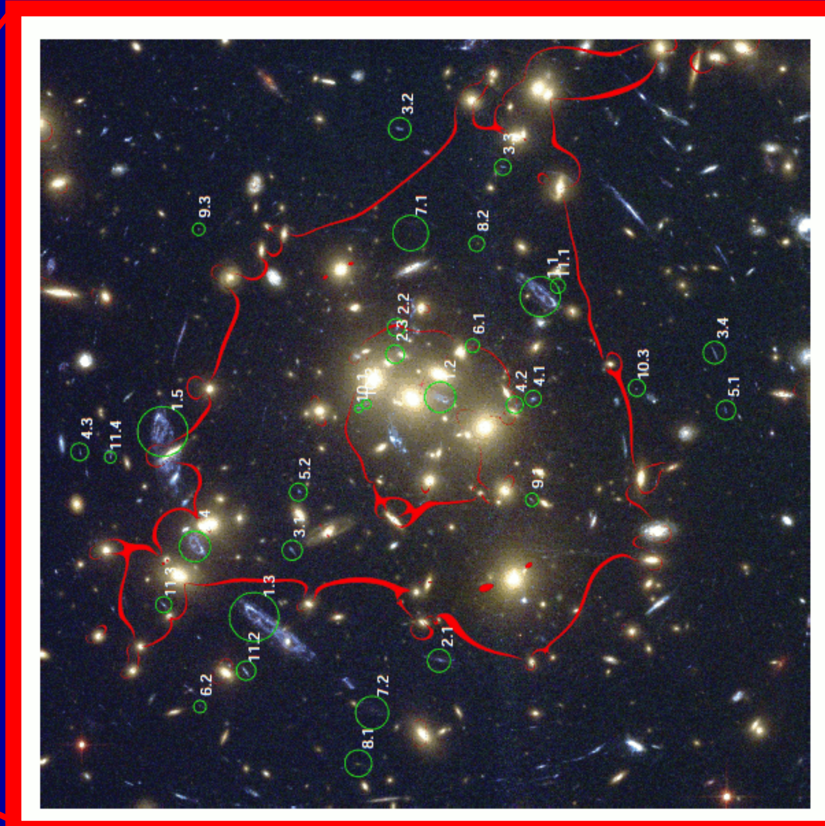

SUBARU/Suprime-Cam (34'x27' FoV)

R_{vir}=~ 1.8Mpc/h (~8 arcmin)

Umetsu et al. 2010, ApJ, arXiv:0908.0069